



**HAL**  
open science

# A New PWM Strategy Based on a 24-Sector Vector Space Decomposition for a Six-Phase VSI-Fed Dual Stator Induction Motor

Khoudir Marouani, Lotfi Baghli, Djafar Hadiouche, Abdelaziz Kheloui,  
Abderrezak Rezzoug

► **To cite this version:**

Khoudir Marouani, Lotfi Baghli, Djafar Hadiouche, Abdelaziz Kheloui, Abderrezak Rezzoug. A New PWM Strategy Based on a 24-Sector Vector Space Decomposition for a Six-Phase VSI-Fed Dual Stator Induction Motor. IEEE Transactions on Industrial Electronics, 2008, 55 (5), pp.1910-1920. 10.1109/TIE.2008.918486 . hal-03562597

**HAL Id: hal-03562597**

**<https://hal.univ-lorraine.fr/hal-03562597>**

Submitted on 9 Feb 2022

**HAL** is a multi-disciplinary open access archive for the deposit and dissemination of scientific research documents, whether they are published or not. The documents may come from teaching and research institutions in France or abroad, or from public or private research centers.

L'archive ouverte pluridisciplinaire **HAL**, est destinée au dépôt et à la diffusion de documents scientifiques de niveau recherche, publiés ou non, émanant des établissements d'enseignement et de recherche français ou étrangers, des laboratoires publics ou privés.

# A New PWM Strategy Based on a 24-Sector Vector Space Decomposition for a Six-Phase VSI-Fed Dual Stator Induction Motor

Khoudir Marouani, Lotfi Baghli, Djafar Hadiouche, Abdelaziz Kheloui, and Abderrezak Rezzoug

**Abstract**—This paper presents a new space vector pulsewidth modulation (SVPWM) technique for the control of six-phase voltage source inverter (VSI)-fed dual stator induction machines (DSIM). A DSIM is an induction machine which has two sets of three-phase stator windings spatially shifted by 30 electrical degrees and fed by two three-phase VSIs. Despite their advantage of power segmentation, these machines are characterized by large zero sequence harmonic currents, and in particular those of order  $6k \pm 1$ , which are due to the mutual cancellation between the two stator windings. The proposed SVPWM scheme, while easy to implement digitally, reduces significantly these extra stator harmonic currents. Experimental results, collected from a 15 kW prototype machine controlled by a digital signal processor are presented and discussed.

**Index Terms**—Dual stator induction machines (DSIM), six-phase voltage source inverter (VSI), space vector pulsewidth modulation (SVPWM).

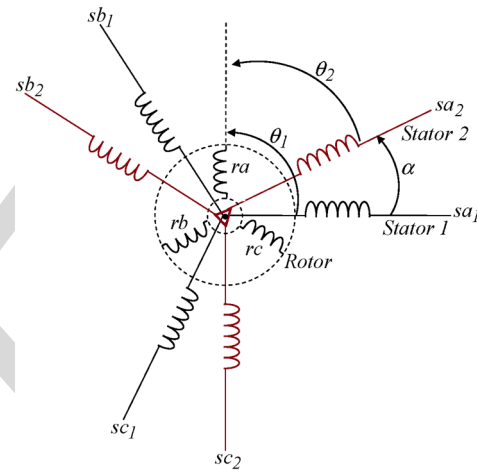


Fig. 1. DSIM windings.

## I. INTRODUCTION

NOWADAYS, electrical machine drives are widely used in industrial applications and transportation systems such as electric/hybrid vehicles, traction locomotives and electric propulsion ships, where high-power levels in conjunction with high-performance requirements are more and more demanded. To achieve these high ratings, there are two possible approaches; one focuses on the converter side by increasing the number of output voltage levels and the other one on the machine side by increasing the number of phases. In the first approach, the idea is to divide the high dc bus voltage into multiple low levels and therefore to distribute the high power required among cells of reduced-voltage power switches without the problem of dynamic voltage sharing encountered in the series connection of active devices. However, increasing the number of inverter levels adds to the control complexity and may introduce some voltage imbalance problems [1]–[3]. It is a solution well suited for high-power and high-voltage utility ap-

plications. For adjustable speed drives, however, an alternative approach is to use a multiphase machine, i.e., a machine with more than three phases in the stator, since the number of phases is not imposed anyway, given that the machine is connected to the electric supply through a dc/ac converter. The number of phases could be used instead as an additional degree of freedom in the overall system design [4].

Although the answer to the question whether it is better to use a multilevel inverter-fed three-phase machine or a multiphase machine depends on the application, it is undeniable that the latter option offers several advantages which may make it appear very attractive. In fact, the most significant features are a low torque ripple, a reduction in the power per phase and fault-tolerance capability. Other interesting advantages can be pointed out, such as a better torque production per ampere for the same machine volume, higher efficiency and improved reliability [5], [6].

A common type of multiphase machine is the dual stator induction machine (DSIM), where two sets of three-phase windings, spatially phase shifted by 30 electrical degrees, share a common stator magnetic core as shown in Fig. 1.

Due to the development of fast switching power semiconductor devices, voltage source inverters (VSIs) are preferred in variable speed machine drives. As VSI-fed multiphase machines are gaining increasing interest for high-power applications, various pulsewidth modulation (PWM) techniques have been developed accordingly, as they strongly affect the overall inverter efficiency and output voltage waveform quality.

Manuscript received February 28, 2007; revised September 24, 2007.

K. Marouani and A. Kheloui are with the Electrical Engineering Laboratory, Polytechnic Military School, 16111 Algiers, Algeria (e-mail: marouani\_khoudir@yahoo.fr; akheloui@caramail.com).

L. Baghli and A. Rezzoug are with the Groupe de Recherche en Electrotechnique et Electronique de Nancy, CNRS UMR 7037, Université Henri Poincaré, 54506 Nancy Cedex, France (e-mail: lotfi.baghli@green.uhp-nancy.fr; abderrezak.rezzoug@green.uhp-nancy.fr).

D. Hadiouche is with the GE Fanuc Automation Solutions Europe, 6468 Echternach, Luxembourg (e-mail: djafar.hadiouche@wanadoo.fr).

Color versions of one or more of the figures in this paper are available online at <http://ieeexplore.ieee.org>.

Digital Object Identifier 10.1109/TIE.2008.918486

68 In a VSI-fed DSIM, the two stator windings are mutually  
69 coupled and small unbalances in the two supply voltages may  
70 generate high currents [7]. Furthermore, because of the low  
71 impedance seen by the voltage harmonic components generated  
72 by the switched voltage waveforms, harmonic currents of high  
73 level are circulating uselessly in the two stator windings, adding  
74 to the overall losses and therefore to the semiconductor devices  
75 ratings [8], [9].

76 To minimize these extra harmonic currents in a six-phase  
77 VSI-fed DSIM, a new 24-sector PWM technique is proposed  
78 in this paper and tested on a 15 kW laboratory machine. The  
79 digital implementation is carried out on a DS1104 dSPACE  
80 controller board. A comparative study between the proposed  
81 technique and similar space vector PWM (SVPWM) techniques  
82 [5], [10], based on analytical harmonic current analysis, is also  
83 developed and discussed.

## 84 II. MACHINE MODEL

85 The machine model is based on the assumption that space  
86 harmonics and magnetic saturation are negligible, and that the  
87 two stator three-phase windings are identical and symmetrical  
88 with the two neutrals being isolated. In order to derive a prac-  
89 tical model suitable for control, a decoupling transformation  
90 matrix is used, as proposed in [5]–[7]. The matrix has the  
91 following form:

$$[T_s]^{-1} = \frac{1}{\sqrt{3}} \begin{bmatrix} 1 & -\frac{1}{2} & -\frac{1}{2} & \frac{\sqrt{3}}{2} & -\frac{\sqrt{3}}{2} & 0 \\ 0 & \frac{\sqrt{3}}{2} & -\frac{\sqrt{3}}{2} & \frac{1}{2} & \frac{1}{2} & -1 \\ \hline 1 & -\frac{1}{2} & -\frac{1}{2} & -\frac{\sqrt{3}}{2} & \frac{\sqrt{3}}{2} & 0 \\ 0 & -\frac{\sqrt{3}}{2} & \frac{\sqrt{3}}{2} & \frac{1}{2} & \frac{1}{2} & -1 \\ \hline 1 & 1 & 1 & 0 & 0 & 0 \\ 0 & 0 & 0 & 1 & 1 & 1 \end{bmatrix}. \quad (1)$$

92 By applying (1) to the voltage vector equations, the overall  
93 machine model is transformed into three decoupled submodels,  
94 written in three independent space coordinates, identified as  
95  $(\alpha-\beta)$ ,  $(x-y)$ , and  $(o_1-o_2)$ , respectively.

96 The machine voltage submodel in  $(\alpha-\beta)$  coordinates can be  
97 written as:

$$\begin{bmatrix} v_{s\alpha} \\ v_{s\beta} \\ v_{r\alpha} \\ v_{r\beta} \end{bmatrix} = \begin{bmatrix} R_s & 0 & 0 & 0 \\ 0 & R_s & 0 & 0 \\ 0 & M\dot{\theta} & R_r & L_r\dot{\theta} \\ -M\dot{\theta} & 0 & -L_r\dot{\theta} & R_r \end{bmatrix} \begin{bmatrix} i_{s\alpha} \\ i_{s\beta} \\ i_{r\alpha} \\ i_{r\beta} \end{bmatrix} + \begin{bmatrix} L_s & 0 & M & 0 \\ 0 & L_s & 0 & M \\ M & 0 & L_r & 0 \\ 0 & M & 0 & L_r \end{bmatrix} \frac{d}{dt} \begin{bmatrix} i_{s\alpha} \\ i_{s\beta} \\ i_{r\alpha} \\ i_{r\beta} \end{bmatrix} \quad (2)$$

98 where  $\dot{\theta} = \Omega_m$  is the rotor mechanical speed, and  $L_s = L_{ls} +$   
99  $3L_{ms}$ ,  $L_r = L_{lr} + (3/2)L_{mr}$ ,  $M = (3/\sqrt{2})M_{sr}$ .  $L_{ls}$  and  $L_{lr}$   
100 are the stator and rotor leakage inductances in  $(\alpha-\beta)$  coordi-  
101 nates, respectively.

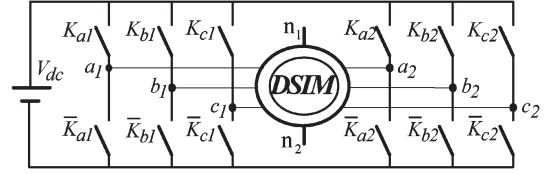


Fig. 2. Six-phase VSI fed DSIM.

The DSIM  $(\alpha-\beta)$  submodel expressed in the stationary  
reference frame is similar to the three-phase induction machine  
model [11].

The machine voltage submodel in  $(x-y)$  coordinates is  
given by:

$$\begin{bmatrix} v_{sx} \\ v_{sy} \end{bmatrix} = \begin{bmatrix} R_s & 0 \\ 0 & R_s \end{bmatrix} \begin{bmatrix} i_{sx} \\ i_{sy} \end{bmatrix} + \begin{bmatrix} L_{lsxy} & 0 \\ 0 & L_{lsxy} \end{bmatrix} \frac{d}{dt} \begin{bmatrix} i_{sx} \\ i_{sy} \end{bmatrix} \quad (3)$$

where  $L_{lsxy}$  is the transformed stator leakage inductance in  
 $(x-y)$  coordinates.

The machine voltage submodel in  $(o_1-o_2)$  coordinates is  
expressed as follows:

$$\begin{bmatrix} v_{so1} \\ v_{so2} \\ v_{ro} \end{bmatrix} = \begin{bmatrix} R_s & 0 & 0 \\ 0 & R_s & 0 \\ 0 & 0 & R_r \end{bmatrix} \begin{bmatrix} i_{so1} \\ i_{so2} \\ i_{ro} \end{bmatrix} + \begin{bmatrix} L_{lso} & 0 & 0 \\ 0 & L_{lso} & 0 \\ 0 & 0 & L_{lr} \end{bmatrix} \frac{d}{dt} \begin{bmatrix} i_{so1} \\ i_{so2} \\ i_{ro} \end{bmatrix} \quad (4)$$

where  $L_{lso}$  is the transformed stator leakage inductance in  
 $(o_1-o_2)$  coordinates.

The electromagnetic torque of the DSIM is expressed only  
in terms of stator and rotor  $(\alpha-\beta)$  current components, since  
the  $(x-y)$  and  $(o_1-o_2)$  counterparts do not contribute to the  
electromechanical energy conversion, as shown by (3) and (4).  
The expression of the electromagnetic torque is then as follows:

$$T_e = pM(i_{s\beta}i_{r\alpha} - i_{s\alpha}i_{r\beta}) \quad (5)$$

where  $p$  is the number of pole pairs.

### General Remarks

The  $(x-y)$  and  $(o_1-o_2)$  current components do not con-  
tribute to the air-gap flux linkages. Hence, they are limited only  
by the stator resistance and leakage inductance [12], [13]. They  
produce only losses and therefore must be kept equal to zero or  
as small as possible.

The transformed voltage equations in the three subframes  
are well decoupled and, as a result, both machine analysis and  
control are greatly simplified.

## III. SVPWM CONTROL OF A DOUBLE-STAR INDUCTION MOTOR

The drive system is a six-phase VSI fed DSIM, as shown  
in Fig. 2. A combinatorial analysis of the inverter switch  
states shows 64 switching modes. Thus, 64 different voltage  
vectors can be applied to the machine. Each voltage vector is  
represented by a decimal number corresponding to the binary  
number  $(K_{c2}K_{b2}K_{a2}K_{c1}K_{b1}K_{a1})$ , which gives the state of

136 the upper switches. By using the  $(6 \times 6)$  transformation matrix  
 137  $[Ts]^{-1}$ , each voltage vector can be decomposed into  $(\alpha-\beta)$ ,  
 138  $(x-y)$ , and  $(o_1-o_2)$  voltages. The  $(o_1-o_2)$  ones are all equal  
 139 to zero because the neutrals  $(n_1, n_2)$  of the two winding sets  
 140 are isolated. So the SVPWM strategy operates in two complex  
 141 planes  $(\alpha-\beta)$  and  $(x-y)$ . Four variables need to be controlled  
 142 simultaneously during each sampling period, by generating  
 143 maximum  $(\alpha-\beta)$  and minimum  $(x-y)$  voltage amplitudes.  
 144 Therefore, during each sampling period, a set of four active  
 145 voltage vectors must be chosen to fulfil these two conditions,  
 146 according to the reference voltage vector location. There are  
 147 numerous ways for choosing such a set.

148 A. Six-Phase SVPWM Techniques

149 The principle of the PWM control techniques proposed in  
 150 [5] and [10] is to choose switching sequences in such a way  
 151 that two consecutive nonzero voltage vectors are practically  
 152 opposite in phase in the  $(x-y)$  plane. In this way, each change  
 153 in the applied vectors leads to a sequence of increases and  
 154 decreases in  $(x-y)$  currents around zero. Moreover, in order  
 155 to minimize  $(x-y)$  harmonic currents and maintain the lowest  
 156 switching frequency, there are different choices to allocate  
 157 zero voltage vectors (0, 7, 56 or 63) within the switching  
 158 sequences. Thus, the switching sequences presented in [10] lead  
 159 to continuous and discontinuous modulation techniques and,  
 160 consequently, to different harmonic distortion characteristics.  
 161 A modulation technique is continuous when on/off switching  
 162 occurs within every sampling period, for all inverter legs and  
 163 all sectors. A modulation technique is discontinuous when one  
 164 (or more) inverter leg stops switching, i.e., the corresponding  
 165 phase voltage is clamped to the positive or negative dc bus for  
 166 at least one sector [14].

167 B. 12-Sector SVPWM Technique

168 In the SVPWM technique addressed in [5], only the  $(\alpha-\beta)$   
 169 voltage vectors having maximum magnitude (45, 41, 9, 11,  
 170 27, 26, 18, 22, 54, 52, 36, 37) are employed to synthesize  
 171 the reference voltage vector  $v_{s\alpha\beta}^*$ . These voltage vectors divide  
 172 the  $(\alpha-\beta)$  plane into 12 sectors and each sector is  $\pi/6$  rad,  
 173 as shown in Fig. 3. For example, voltage vectors 45, 41, 9,  
 174 and 11 are selected when the reference voltage vector is located  
 175 in sector 1. As shown in Fig. 4, continuous and discontinuous  
 176 modulation techniques can be obtained according to the switch-  
 177 ing sequences given below.

178 1) Continuous Modulation C6  $\phi$  SVPWM12: For example,  
 179 when the reference voltage vector is located in sector 1, a con-  
 180 tinuous modulation technique (C6  $\phi$  SVPWM12) is obtained  
 181 with the following sequence:

$$|7-45-41-56-9-11-7|7-11-9-56-41-45-7|.$$

182 2) Discontinuous Modulation D6  $\phi$  SVPWM12-A: For the  
 183 same sector 1, a discontinuous modulation technique (D6  $\phi$   
 184 SVPWM12-A) can be obtained with the following sequence:

$$|7-45-41-9-11-7|7-11-9-41-45-7|.$$

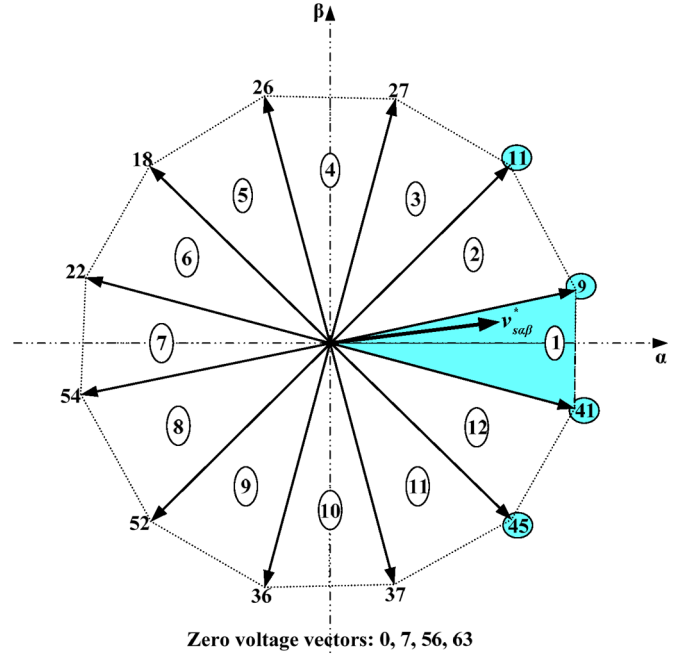


Fig. 3. Presentation of the inverter voltage vectors having maximum magnitude in  $(\alpha-\beta)$  plane.

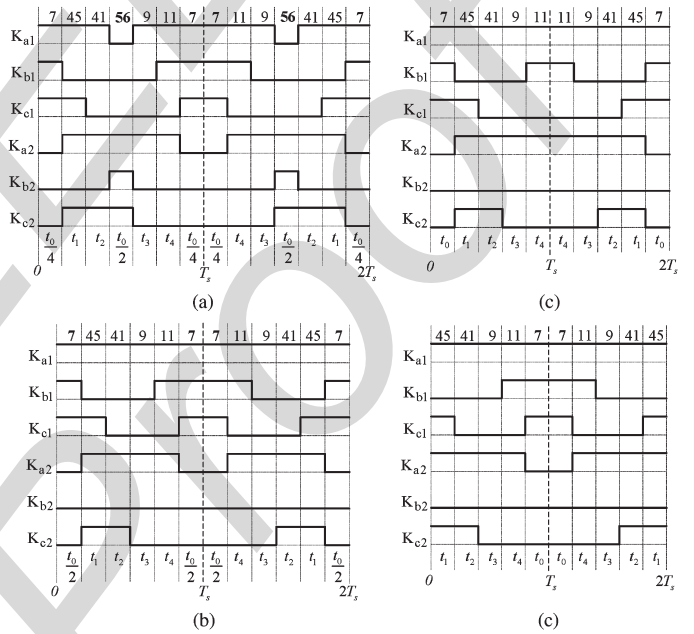


Fig. 4. Twelve-sector SVPWM switching sequences when the reference voltage vector is located in sector 1. (a) C6  $\phi$  SVPWM12. (b) D6  $\phi$  SVPWM12-A. (c) D6  $\phi$  SVPWM12-B1. (d) D6  $\phi$  SVPWM12-B2.

3) Discontinuous Modulation D6  $\phi$  SVPWM12-B1: In the 185  
 D6  $\phi$  SVPWM12-B1, the zero-voltage vectors are applied at the 186  
 beginning and at the end of the switching sequence as follows: 187

$$|7-45-41-9-11|11-9-41-45-7|.$$

4) Discontinuous Modulation D6  $\phi$  SVPWM12-B2: In the 188  
 D6  $\phi$  SVPWM12-B2, the zero-voltage vectors are applied in 189  
 the middle of the switching sequence as follows: 190

$$|45-41-9-11-7|7-11-9-41-45|.$$

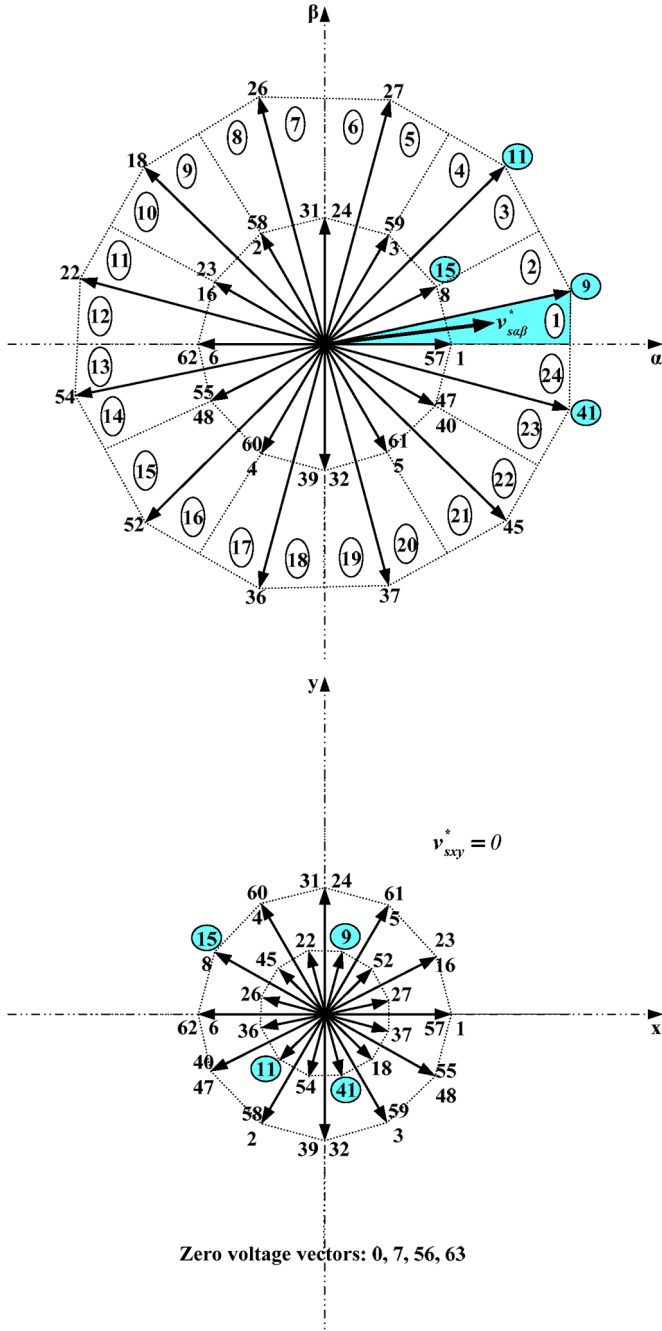


Fig. 5. Presentation of the inverter voltage vectors having maximum and half magnitude in  $(\alpha-\beta)$ , and  $(x-y)$  planes.

### 191 C. Proposed 24-Sector SVPWM Technique

192 As shown in Fig. 4, the switching pattern corresponding  
 193 to the switching sequences of the 12-sector PWM techniques  
 194 presents asymmetrical waveforms and usually more than two  
 195 transitions (from low to high or from high to low) occur on  
 196 the corresponding PWM outputs within a sampling period,  
 197 which increases the switching frequency of the inverter legs  
 198 and causes difficulties for digital signal processor (DSP) im-  
 199 plementation of these strategies. Accordingly, some additional  
 200 adaptations in DSP programs are necessary to ensure successful  
 201 experiments [15], [16].

202 To overcome these drawbacks, the new 24-sector SVPWM  
 203 technique proposed in this paper combines the maximum

magnitude  $(\alpha-\beta)$  voltage vectors and the ones with half  
 204 magnitude (1, 57, 8, 15, 3, 59, 24, 31, 2, 58, 16, 23, 6, 205  
 62, 48, 55, 4, 60, 32, 39, 5, 61, 40, 47) generated by one 206  
 inverter. These voltage vectors divide the  $(\alpha-\beta)$  plane into 207  
 twenty four  $\pi/12$ -rad sectors, as shown in Fig. 5. In each 208  
 sampling period, the reference voltage vector is achieved by 209  
 selecting a set of three voltage vectors among those having 210  
 maximum magnitude and a fourth vector among the ones with 211  
 half magnitude. For example, voltage vectors 41, 9, 11 and 15 212  
 are selected when the reference voltage vector is located in 213  
 sector 1. Then, the voltage vectors applying times:  $t_1, t_2, t_3$  and 214  
 $t_4$  are obtained as explained in Appendix A. For the remaining 215  
 time  $t_0 = T_s - (t_1 + t_2 + t_3 + t_4)$ , zero state vectors (0, 7, 56 216  
 or 63) are applied. Consequently, simple PWM outputs with 217  
 symmetrical waveforms are obtained. As shown in Fig. 6, 218  
 only two transitions or less (from low to high or from high 219  
 to low) occur on the corresponding PWM outputs within a 220  
 sampling period. This fact decreases the switching frequency 221  
 of the inverter legs and allows easy DSP implementation. The 222  
 switching sequences and the corresponding applying times for 223  
 all sectors are presented in Table I. It should also be noticed 224  
 that both continuous and discontinuous modulation techniques 225  
 can be obtained with this new 24-sector SVPWM scheme. This 226  
 is achieved by selecting the appropriate zero voltage vector 227  
 locations within the switching sequence. 228

1) *Continuous Modulation C6  $\phi$  SVPWM24*: Continuous 229  
 PWM technique (C6  $\phi$  SVPWM24) can be obtained for all sec- 230  
 tors by selecting the switching sequences presented in Table I. 231  
 As an example, when the reference voltage vector is located 232  
 in sector 1, a C6  $\phi$  SVPWM24 is obtained by selecting the 233  
 following sequence: 234

$$|56-41-9-11-15-7|7-15-11-9-41-56|.$$

2) *Discontinuous Modulation D6  $\phi$  SVPWM24-B1 and B2*: 235  
 Two discontinuous PWM schemes can be obtained through the 236  
 appropriate positioning of the zero voltage vectors. In sector 1, 237  
 the examples are as follows. 238

1) D6  $\phi$  SVPWM24-B1: The first discontinuous modulation 239  
 technique can be obtained by placing the zero voltage 240  
 vector both at the beginning and at the end of the switch- 241  
 ing sequence, as follows: 242

$$|56-41-9-11-15|15-11-9-41-56|.$$

2) D6  $\phi$  SVPWM24-B2: The second discontinuous mod- 243  
 ulation technique is obtained by placing the zero volt- 244  
 age vector in the middle of the switching sequence, as 245  
 follows: 246

$$|41-9-11-15-7|7-15-11-9-41|.$$

3) *Switching Sequences and Applying Time Selection*: For 247  
 optimal DSP implementation and low algorithm execution time, 248  
 the applying times ( $t_1, t_2, t_3$ , and  $t_4$ ) computation can be 249  
 simplified by an offline calculation for all sectors in the same 250  
 manner as for sector 1. As a result, within each sampling period, 251  
 there is a total of only 12 coefficients  $T_i$  to be calculated in (6). 252

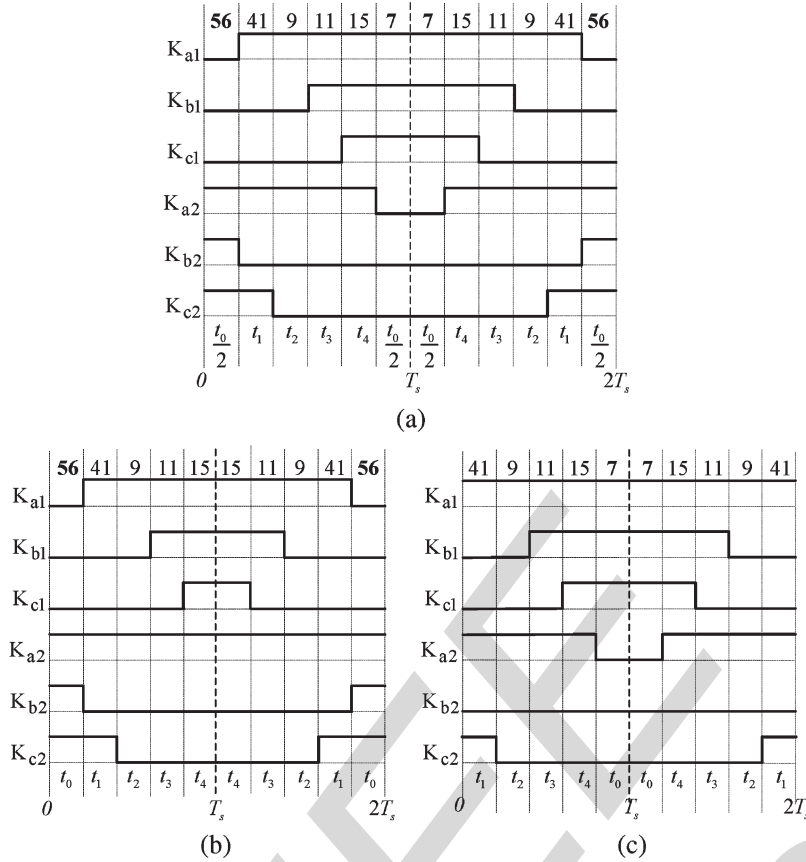


Fig. 6. Twenty-four-sector SVPWM switching sequences when the reference voltage vector is located in sector 1. (a) C6  $\phi$  SVPWM24. (b) D6  $\phi$  SVPWM24-B1. (c) D6  $\phi$  SVPWM24-B2.

253 Table I describes the C6  $\phi$  SVPWM24 switching sequences and  
 254 applying time selection according to the sector number in the  
 255  $(\alpha-\beta)$  plane.

$$\begin{bmatrix} T_1 \\ T_2 \\ T_3 \\ T_4 \\ T_5 \\ T_6 \\ T_7 \\ T_8 \\ T_9 \\ T_{10} \\ T_{11} \\ T_{12} \end{bmatrix} = \frac{T_s}{2V_{dc}} \begin{bmatrix} \sqrt{3}-2 & 1 \\ 1 & -\sqrt{3} \\ 1 & \sqrt{3}-2 \\ 0 & 2 \\ \sqrt{3}-1 & \sqrt{3}-1 \\ -(\sqrt{3}-1) & \sqrt{3}-1 \\ \sqrt{3} & -1 \\ 1 & -(\sqrt{3}-2) \\ -(\sqrt{3}-2) & 1 \\ 2 & 0 \\ \sqrt{3} & 1 \\ 1 & \sqrt{3} \end{bmatrix} \begin{bmatrix} v_{s\alpha}^* \\ v_{s\beta}^* \end{bmatrix}. \quad (6)$$

#### 256 D. Maximum Modulation Index

257 The modulation index  $m$  can be defined as the ratio of  
 258 the fundamental component magnitude of the line to neutral  
 259 inverter output voltage  $V_{1m}$  to the fundamental component  
 260 magnitude of the six-step mode voltage  $V_{1m6step} = 2V_{dc}/\pi$   
 261 [17]. When the inverter is operating in the linear modulation  
 262 region, the sum of the applying times of the active voltage  
 263 vectors is less than the switching period  $T_s$  [18], [19]. The  
 264 largest value for linear output with the 12-sector and the  
 265 proposed 24-sector SVPWM techniques,  $m_{max} = \pi/(2\sqrt{3}) \approx$

0.907, coincides with the corresponding value for the three-  
 266 phase SVPWM [20]. Note that  $m_{max}$  is obtained by solving  
 267  $t_0 = T_s - (t_1 + t_2 + t_3 + t_4) = 0$  as shown in Appendix B. 268

#### IV. HARMONIC CURRENT ANALYSIS

269

The voltage and current waveform quality of the PWM-VSI  
 270 drives is determined via the switching frequency harmonics,  
 271 since they determine the switching frequency copper losses  
 272 and the torque ripple of a motor load and the line current  
 273 total harmonic distortion of a line-connected VSI. While the  
 274 copper losses are measured over a fundamental cycle and  
 275 therefore require a per fundamental cycle (macroscopic) rms  
 276 ripple current value calculation, the peak and local stresses  
 277 are properly investigated on a per-carrier cycle (microscopic)  
 278 basis. Therefore, first a microscopic and then a macroscopic  
 279 investigation is required [20]. Because, the machine model  
 280 includes  $(\alpha-\beta)$  and  $(x-y)$  components, the harmonic current  
 281 analysis must be made for the  $(\alpha-\beta)$  and  $(x-y)$  currents. 282

#### A. Normalized Harmonic Currents and Fluxes Calculation

283

The stator voltage equations in the stator coordinate system  
 284 are expressed as follows: 285

$$\begin{aligned} v_{s\alpha\beta} &= R_s i_{s\alpha\beta} + \frac{d\lambda_{s\alpha\beta}}{dt} \\ v_{sxy} &= R_s i_{sxy} + L_{lsxy} \frac{di_{sxy}}{dt} \end{aligned} \quad (7)$$

TABLE I  
PROPOSED C6  $\phi$  SVPWM24 SWITCHING SEQUENCES

Sector	Switching sequences	Voltage vectors applying times			
		$t_1$	$t_2$	$t_3$	$t_4$
1	56-41-9-11-15-7	$T_2$	$T_5$	$T_4$	$-T_1$
2	56-57-41-9-11-7	$T_1$	$T_2$	$T_3$	$T_4$
3	0-9-11-27-59-63	$T_7$	$T_9$	$-T_2$	$-T_6$
4	0-8-9-11-27-63	$T_6$	$T_7$	$T_8$	$-T_2$
5	7-11-27-26-24-56	$T_{10}$	$T_1$	$-T_7$	$T_3$
6	7-3-11-27-26-56	$-T_3$	$T_{10}$	$T_5$	$-T_7$
7	63-27-26-18-2-0	$T_{11}$	$T_6$	$-T_{10}$	$T_8$
8	63-31-27-26-18-0	$-T_8$	$T_{11}$	$T_9$	$-T_{10}$
9	56-26-18-22-23-7	$T_{12}$	$-T_3$	$-T_{11}$	$T_5$
10	56-58-26-18-22-7	$-T_5$	$T_{12}$	$T_1$	$-T_{11}$
11	0-18-22-54-62-63	$T_4$	$-T_8$	$-T_{12}$	$T_9$
12	0-16-18-22-54-63	$-T_9$	$T_4$	$T_6$	$-T_{12}$
13	7-22-54-52-48-56	$-T_2$	$-T_5$	$-T_4$	$T_1$
14	7-6-22-54-52-56	$-T_1$	$-T_2$	$-T_3$	$-T_4$
15	63-54-52-36-4-0	$-T_7$	$-T_9$	$T_2$	$T_6$
16	63-55-54-52-36-0	$-T_6$	$-T_7$	$-T_8$	$T_2$
17	56-52-36-37-39-7	$-T_{10}$	$-T_1$	$T_7$	$-T_3$
18	56-60-52-36-37-7	$T_3$	$-T_{10}$	$-T_5$	$T_7$
19	0-36-37-45-61-63	$-T_{11}$	$-T_6$	$T_{10}$	$-T_8$
20	0-32-36-37-45-63	$T_8$	$-T_{11}$	$-T_9$	$T_{10}$
21	7-37-45-41-40-56	$-T_{12}$	$T_3$	$T_{11}$	$-T_5$
22	7-5-37-45-41-56	$T_5$	$-T_{12}$	$-T_1$	$T_{11}$
23	63-45-41-9-1-0	$-T_4$	$T_8$	$T_{12}$	$-T_9$
24	63-47-45-41-9-0	$T_9$	$-T_4$	$-T_6$	$T_{12}$

286 where the stator and the rotor flux equations are given by:

$$\begin{aligned}\lambda_{s\alpha\beta} &= L_s i_{s\alpha\beta} + M i_{r\alpha\beta} \\ \lambda_{r\alpha\beta} &= L_r i_{r\alpha\beta} + M i_{s\alpha\beta}.\end{aligned}\quad (8)$$

287 The stator flux equation can be rewritten as:

$$\lambda_{s\alpha\beta} = \sigma L_s i_{s\alpha\beta} + \frac{M}{L_r} \lambda_{r\alpha\beta}.\quad (9)$$

288 Substituting (9) in (7), the stator voltage equation can be  
289 expressed as follows:

$$v_{s\alpha\beta} = R_s i_{s\alpha\beta} + \sigma L_s \frac{di_{s\alpha\beta}}{dt} + \frac{M}{L_r} \frac{d\lambda_{r\alpha\beta}}{dt}.\quad (10)$$

290 If only the harmonic voltages and currents are considered,  
291 it will be assumed that the reference voltage vector  $v_{s\alpha\beta}^*$  is  
292 constant over the switching period  $T_s$ , because the switching  
293 frequency  $f_s$  is much higher than the fundamental frequency  
294  $f_e$ , and that the stator and the rotor time constants are much  
295 larger than the switching period, with the resistance drops being  
296 neglected [21]. Under these assumptions, the voltages and

currents can be separated in the harmonic components, which  
change over  $T_s$  while the fundamental components remain  
constant over the same period. Thus, from (7) and (10), the  
harmonic voltage equations can be expressed as follows:

$$\begin{aligned}\tilde{v}_{s\alpha\beta} &= \sigma L_s \frac{d\tilde{i}_{s\alpha\beta}}{dt} \\ \tilde{v}_{sxy} &= L_{lsxy} \frac{d\tilde{i}_{sxy}}{dt}\end{aligned}\quad (11)$$

where  $\tilde{v}_{s\alpha\beta}$  is the harmonic voltage and is equal to the  
difference between the actual voltage vector and the reference  
vector  $v_{s\alpha\beta}^*$ .

Assuming that the instantaneous harmonic currents are zero  
at the beginning and at the end of the carrier cycle, the  
( $\alpha-\beta$ ) and ( $x-y$ ) harmonic stator currents per-carrier cycle can be  
calculated as follows [20], [22], [23]:

$$\begin{aligned}\tilde{i}_{s\alpha\beta} &= \frac{1}{\sigma L_s} \int_{NT_s}^{(N+1)T_s} (V_{s\alpha\beta k} - v_{s\alpha\beta}^*) dt \\ \tilde{i}_{sxy} &= \frac{1}{L_{lsxy}} \int_{NT_s}^{(N+1)T_s} (V_{sxy k}) dt.\end{aligned}\quad (12)$$

In (12),  $V_{s\alpha\beta k}$  and  $V_{sxy k}$  are the inverter output voltage  
vectors of the  $k$ th state. They change according to the selected  
switching sequence, since for high  $f_s/f_e$  values, the  $v_{s\alpha\beta}^*$  term  
can be assumed as constant within a carrier cycle. Thus, the  
above integral can be calculated in a closed form.

Because the harmonic current and harmonic flux are only  
different in scale, and in order to eliminate the need for  
load parameters in (12), the harmonic flux trajectories can  
be investigated. Nevertheless, the ( $x-y$ ) current components  
are limited by the stator leakage inductance  $L_{lsxy}$ , which de-  
pends on the coil pitch of the stator windings [10]. Conse-  
quently, the harmonic characteristics of the VSI feeding DSIM  
should be investigated with the introduction of the coefficient  
 $k_{\sigma xy} = \sigma L_s / L_{lsxy}$ , which is necessary to evaluate and com-  
pare the performances of the PWM techniques. So, employ-  
ing (12) and normalizing with respect to  $\lambda_b$ , the per-carrier  
cycle rms value of the normalized harmonic current can be  
calculated with:

$$\begin{aligned}\tilde{i}_{srms}^2(m, \theta) &= \left(\frac{\lambda_b}{\sigma L_s}\right)^2 \frac{1}{T_s} \int_{NT_s}^{(N+1)T_s} \left(\tilde{\lambda}_{s\alpha\beta}^2 + k_{\sigma xy}^2 \tilde{\lambda}_{sxy}^2\right) dt \\ &= \left(\frac{\lambda_b}{\sigma L_s}\right)^2 \left(\tilde{\lambda}_{s\alpha\beta rms}^2(m, \theta) + k_{\sigma xy}^2 \tilde{\lambda}_{sxy rms}^2(m, \theta)\right) \\ &= \left(\frac{\lambda_b}{\sigma L_s}\right)^2 \left(\tilde{\lambda}_{srms}^2(m, \theta)\right)\end{aligned}\quad (13)$$

where  $\lambda_b = 2\sqrt{3}V_{dc}T_s/\pi$ ,  $\tilde{\lambda}_{s\alpha\beta} = \sigma L_s \tilde{i}_{s\alpha\beta}$ , and  $\tilde{\lambda}_{sxy} =$   
 $L_{lsxy} \tilde{i}_{sxy}$

TABLE II  
SWITCHING FREQUENCY REDUCTION COEFFICIENT

N°	SVPWM Techniques	$k_f$	$f_s$
1	C6 $\phi$ SVPWM12	1	
2	D6 $\phi$ SVPWM12-A	2/3	
3	D6 $\phi$ SVPWM12-B1	1/2	
4	D6 $\phi$ SVPWM12-B2	5/12	$f_s = \frac{1}{k_f} \cdot f_{sw}$
5	C6 $\phi$ SVPWM24	1	
6	D6 $\phi$ SVPWM24-B1	5/6	
7	D6 $\phi$ SVPWM24-B2	2/3	

The per-fundamental cycle rms value of the harmonic current determines the waveform quality and harmonic losses. Averaging (13) over a fundamental period results in the global harmonic current calculation as follows:

$$\begin{aligned}
 \tilde{I}_{sfrms}^2(m) &= \left( \frac{\lambda_b}{\sigma L_s} \right)^2 \frac{1}{2\pi} \int_{2\pi} \tilde{\lambda}_{sfrms}^2(m, \theta) d\theta \\
 &= \left( \frac{\lambda_b}{\sigma L_s} \right)^2 \left( \tilde{\lambda}_{s\alpha\beta frms}^2(m) + k_{\sigma xy}^2 \tilde{\lambda}_{sxy frms}^2(m) \right) \\
 &= \left( \frac{\lambda_b}{\sigma L_s} \right)^2 \tilde{\lambda}_{sfrms}^2(m). \quad (14)
 \end{aligned}$$

The above integral yields a polynomial function of the modulation index  $m$ . As an example, the per-fundamental cycle rms normalized harmonic flux  $\tilde{\lambda}_{sfrms}$  was calculated for all the discussed PWM techniques. This results in  $m$  dependent analytical formulas summarized in Appendix C.

### B. Performance Comparison

For comparison purposes, the harmonic current analysis is performed at the same average switching frequency  $f_{sw}$  for all the PWM techniques. Therefore, a switching frequency reduction coefficient  $k_f$  is introduced for each PWM technique according to Table II. This coefficient can be determined from the ratio of the discontinuous to the continuous PWM techniques regarding the number of commutations of all legs during one sampling period. The curves of the per-fundamental cycle normalized rms harmonic flux for all the discussed PWM techniques have been plotted as a function of modulation index  $m$ , as shown in Fig. 7. It is clear that the rms value of the harmonic flux varies with the PWM technique used and according to the selected switching sequences. These curves show that the D6  $\phi$  SVPWM12-A has practically the best performance at a low modulation index range, while the D6  $\phi$  SVPWM12-B1 (B2) exhibits the best performance in the high modulation index range. However, as the modulation index increases, the C6  $\phi$  SVPWM12 performance rapidly degrades compared to the C6  $\phi$  SVPWM24 of the proposed 24-sector PWM scheme, which reveals excellent performance over the whole voltage range. While the D6  $\phi$  SVPWM24-B1-(B2) PWM strategies present harmonic characteristics similar to the ones obtained with the D6  $\phi$  SVPWM12-A-(B1) and (B2) strategies, the

proposed 24-sector PWM techniques allow a sampling frequency increase and as a result, the switching frequency can be increased by a factor of two as compared to the 12-sector PWMs. Therefore, significant harmonic current reductions can be achieved as shown in Fig. 7(h) for the worst case, when  $k_{\sigma xy} = 10$ .

It should be noted that discontinuous PWM techniques allow a higher sampling rate selection and can be applied in a high voltage range, while continuous ones are advantageous in the low voltage range. In addition, an optimal PWM scheme can be obtained with a transition between these SVPWM strategies to allow rms harmonic current minimization over the whole voltage range. The intersection points define the optimal transition between different PWM techniques.

Finally, a careful look at D6  $\phi$  SVPWM12-B1 in Fig. 4(c) shows that during one switching period  $T_s$ , two inverter legs have commutations twice. D6  $\phi$  SVPWM12-B2 in Fig. 4(d) shows that one inverter leg has commutations twice. This is never the case for D6  $\phi$  SVPWM24-B1 and B2. Therefore, 12-sector discontinuous PWMs have a maximum instantaneous switching frequency twice as big as in the case of 24-sector discontinuous PWMs. This fact has an impact on inverter switching losses [14], [20]. While it is not the aim of this paper to evaluate the performance of PWM techniques in terms of inverter switching and conduction losses, it can be expected that the 24-sector discontinuous PWMs will have a better performance than the 12-sector ones. Further works on switching and conduction losses are in progress and will be reported in a subsequent paper.

## V. EXPERIMENTAL RESULTS

To confirm the feasibility of the proposed SVPWM techniques over the entire voltage range under  $V/f$  control, a set of experiments are carried out. The experimental test bench (Fig. 8) is composed of a six-phase VSI feeding a 15 kW DSIM prototype, and the whole control algorithm is tested on a dSPACE DS1104 controller board. The original 320F240 firmware does not allow the change in PWM compare registers and action registers many times during a period. So, to allow four changes within PWM period  $T_s$ , the flashed firmware is reprogrammed [15], [24]. Hence, it is possible to implement the 12-sector PWM techniques.

On the contrary, for the proposed 24-sector PWM strategies, usually at most two transitions (from low to high or from high to low) occur symmetrically on the corresponding PWM outputs within a sampling period. This allows easier DSP implementation. Then the original 320F240 firmware is used with the help of specially developed user functions that allow the synchronization of six full PWM and three simple PWM simultaneously on the DS1104 DSP board.

These PWM techniques are successfully tested and the following conclusions can be drawn from these experimental results: In the case of the 12-sector PWM strategies, usually more than two transitions (from low to high or from high to low) occur on the corresponding PWM outputs. This increases the switching frequency of the inverter legs and complicates the experimental test. However, the number of transitions

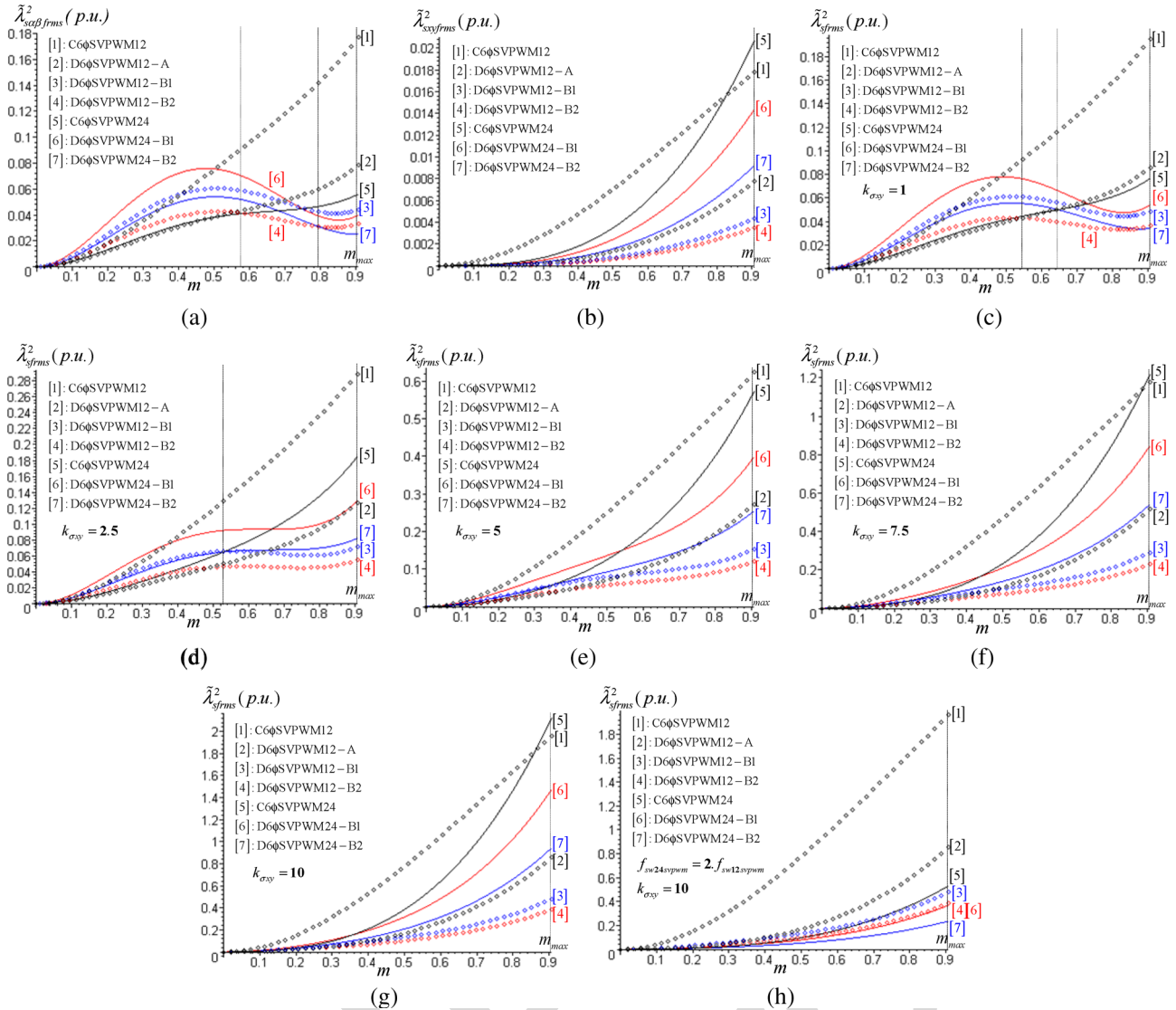


Fig. 7. Per fundamental cycle normalized rms harmonic flux as a function of modulation index  $m$ , for all the discussed PWM techniques. (a)  $(\alpha-\beta)$  rms harmonic flux. (b)  $(x-y)$  rms harmonic flux. (c), (d), (e), (f), (g) RMS harmonic flux at different leakage coupling ( $k_{\sigma xy} = 1; 2.5; 5; 7.5; 10$ ), at the same average switching frequency  $f_{sw}$ . (h) RMS harmonic flux with  $k_{\sigma xy} = 10$ , at  $f_s = 2 \cdot f_{sw}$  for the proposed 24-sector PWM techniques.

417 on the corresponding PWM outputs is reduced in the case  
418 of the proposed 24-sector PWM strategies, which decrease  
419 the switching frequency of the inverter legs and allow easy  
420 DSP implementation. In addition, for discontinuous PWM tech-  
421 niques, at least two PWM outputs remain unchanged during the  
422 entire sampling period. Therefore, the carrier frequency can be  
423 increased with harmonic losses reduction.

424 Experimental results under constant  $V/f$  control, for the  
425 cases of C6  $\phi$  SVPWM12, D6  $\phi$  SVPWM12-B2, C6  $\phi$   
426 SVPWM24, and D6  $\phi$  SVPWM24-B2 techniques are pre-  
427 sented in Fig. 9. The average switching frequency is set to  
428  $f_{sw} = 5$  kHz and the motor is running at 735 r/min with a  
429 connected load. As expected, these SVPWM techniques al-  
430 low the control of the  $(\alpha-\beta)$  and  $(x-y)$  current components  
431 simultaneously.

432 However, these experimental results demonstrate that the  
433 continuous PWM techniques produce a larger amplitude of  
434 the harmonic currents in the  $(x-y)$  plane as compared to  
435 the discontinuous ones where the amplitude of these currents

is minimized. Moreover, the phase current presents a pure  
436 sinusoidal shape and the trajectory of the  $(\alpha-\beta)$  stator cur-  
437 rent components is a circle for all these PWM techniques,  
438 confirming that these currents are controlled as well as  $(x-y)$   
439 harmonic currents. Indeed, it should be remembered that the  
440 carrier frequency can be increased by a factor of two for a 50%  
441 reduction of harmonic losses in the case of C6  $\phi$  SVPWM24,  
442 or by a factor three for a 66% reduction in harmonic losses  
443 with the D6  $\phi$  SVPWM24-B2 technique. In addition, due  
444 to the simplicity and regularity of the proposed 24-sector  
445 PWM techniques, low-cost DSPs for motor control may easily  
446 be used. 447

## VI. CONCLUSION

448  
449 In this paper, a new SVPWM technique based on the vector  
450 space decomposition suitable for six-phase VSI-fed DSIM has  
451 been presented. The switching sequences presented lead to  
452 continuous and discontinuous modulation strategies, according

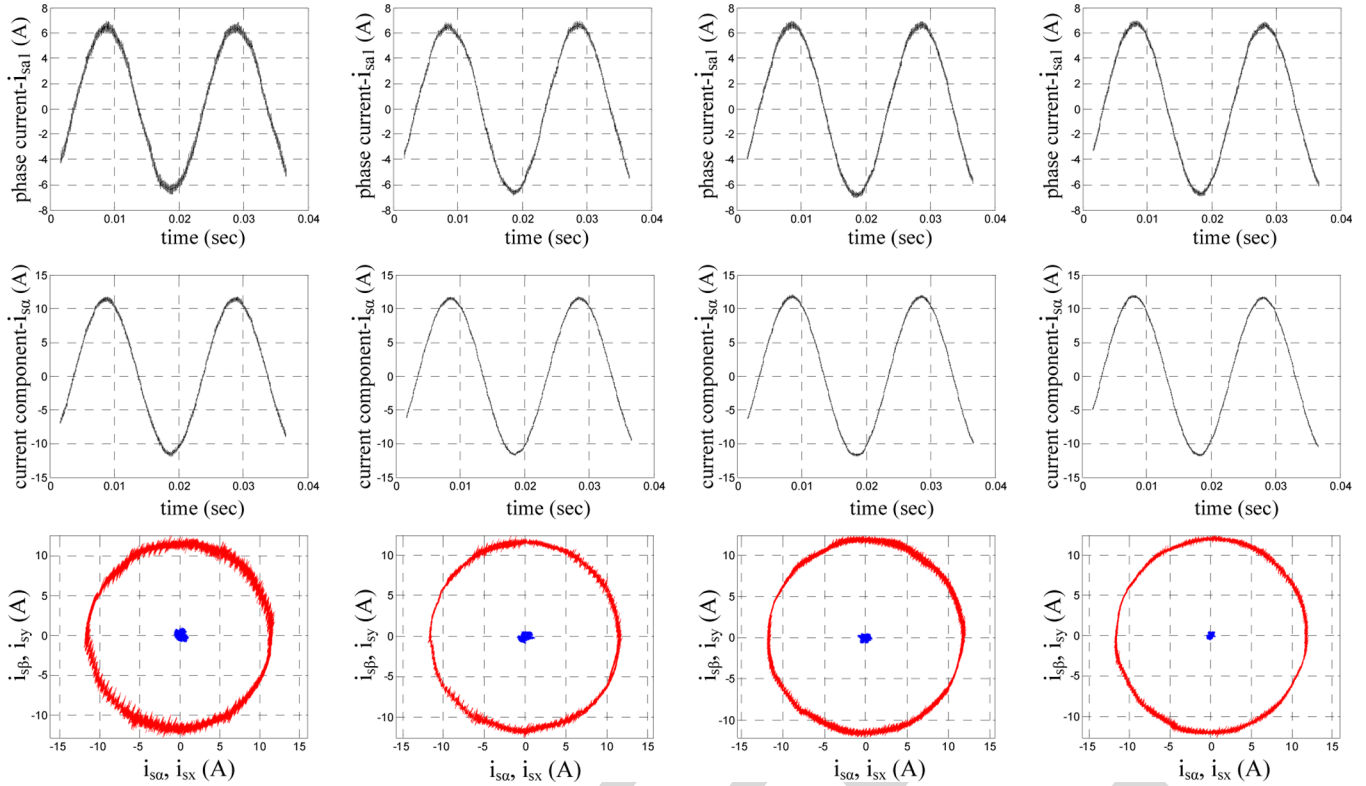


Fig. 8. Experimental test bench.



Fig. 9. Experimental results of the SVPWM techniques with the motor operating under a constant  $V/f$  control with connected load for  $f_e = 50$  Hz, at 735 r/min and for the same average switching frequency  $f_{sw}$ . From top to bottom:  $i_{sa1}$  phase current,  $i_{s\alpha}$  current component,  $(\alpha-\beta)$  and  $(x-y)$  plane current trajectories. From left to right: C6  $\phi$  SVPWM12, D6  $\phi$  SVPWM12-B2, C6  $\phi$  SVPWM24, and D6  $\phi$  SVPWM24-B2.

453 to the position of zero voltage vectors during each sampling  
454 period. It is shown that the harmonic current rms values vary  
455 according to the selected switching sequence and the voltage  
456 range. Likewise, from this point of view, the continuous PWM  
457 technique has an advantage in the low and medium voltage  
458 range, while the discontinuous PWM strategy is advantageous  
459 in the high voltage range. Thus, the combination of these  
460 strategies provides the best harmonic current performance over  
461 the whole voltage range. It has been demonstrated that the pro-  
462 posed 24-sector SVPWM techniques, while easy to implement  
463 digitally, allow a switching frequency increase with significant  
464 extra stator harmonic currents reduction.

## APPENDIX A

465

## VOLTAGE VECTORS APPLYING TIMES CALCULATION

466

The inverter output voltage vectors are represented in Figs. 3, 467  
and Fig. 5 by decimal number  $k$  equivalent to the binary number 468  
formed by the instantaneous values of the switching functions 469  
defined as: 470

$$k = K_{a1} \times 2^0 + K_{b1} \times 2^1 + K_{c1} \times 2^2 + K_{a2} \times 2^3 + K_{b2} \times 2^4 + K_{c2} \times 2^5. \quad (A1)$$

The instantaneous values of the six-phase VSI output voltage 471  
vectors  $(v_{a1}, v_{b1}, v_{c1}, v_{a2}, v_{b2}, v_{c2})$  can be determined by using 472  
the inverter connection matrix  $[Mc]$  as follows: 473

$$[v_{a1} \ v_{b1} \ v_{c1} \ v_{a2} \ v_{b2} \ v_{c2}]^T = [Mc][K_{a1} \ K_{b1} \ K_{c1} \ K_{a2} \ K_{b2} \ K_{c2}]^T \quad (A2)$$

where

474

$$[Mc] = \frac{V_{dc}}{3} \begin{bmatrix} 2 & -1 & -1 & 0 & 0 & 0 \\ -1 & 2 & -1 & 0 & 0 & 0 \\ -1 & -1 & 2 & 0 & 0 & 0 \\ \hline 0 & 0 & 0 & 2 & -1 & -1 \\ 0 & 0 & 0 & -1 & 2 & -1 \\ 0 & 0 & 0 & -1 & -1 & 2 \end{bmatrix}. \quad (A3)$$

The inverter output voltage vectors are transformed into 475  
 $(\alpha-\beta)$ ,  $(x-y)$ , and  $(o_1-o_2)$  planes by means of the transfor- 476  
mation matrix  $[Ts]^{-1}$  given in (1), as: 477

$$[v_{s\alpha k} \ v_{s\beta k} \ v_{sxk} \ v_{syk} \ v_{o1k} \ v_{o2k}]^T = [Ts]^{-1}[v_{a1} \ v_{b1} \ v_{c1} \ v_{a2} \ v_{b2} \ v_{c2}]^T \quad (A4)$$

478 For example, when the reference voltage vector is located in  
479 sector 1, voltage vectors 41, 9, 11, and 15 are selected and their  
480 equivalent binary numbers are defined as:

$$\begin{aligned} 41 &= [1 \ 0 \ 1|0 \ 0 \ 1] \\ 9 &= [0 \ 0 \ 1|0 \ 0 \ 1] \\ 11 &= [0 \ 0 \ 1|0 \ 1 \ 1] \\ 15 &= [0 \ 0 \ 1|1 \ 1 \ 1]. \end{aligned} \quad (\text{A5})$$

481 Then the  $(\alpha-\beta)$ , and  $(x-y)$  voltages can be calculated by  
482 using (A2), and (A4), as follows:

$$\begin{aligned} &\begin{bmatrix} V_{s\alpha 41} & V_{s\alpha 9} & V_{s\alpha 11} & V_{s\alpha 15} \\ V_{s\beta 41} & V_{s\beta 9} & V_{s\beta 11} & V_{s\beta 15} \\ V_{sx 41} & V_{sx 9} & V_{sx 11} & V_{sx 15} \\ V_{sy 41} & V_{sy 9} & V_{sy 11} & V_{sy 15} \end{bmatrix} \\ &= \frac{V_{dc}}{2\sqrt{3}} \begin{bmatrix} 2 + \sqrt{3} & 2 + \sqrt{3} & 1 + \sqrt{3} & \sqrt{3} \\ -1 & 1 & 1 + \sqrt{3} & 1 \\ 2 - \sqrt{3} & 2 - \sqrt{3} & 1 - \sqrt{3} & -\sqrt{3} \\ -1 & 1 & 1 - \sqrt{3} & 1 \end{bmatrix}. \end{aligned} \quad (\text{A6})$$

483 The voltage vectors applying times:  $t_1$ ,  $t_2$ ,  $t_3$  and  $t_4$  are  
484 obtained as:

$$\begin{aligned} \begin{bmatrix} t_1 \\ t_2 \\ t_3 \\ t_4 \end{bmatrix} &= \begin{bmatrix} V_{s\alpha 41} & V_{s\alpha 9} & V_{s\alpha 11} & V_{s\alpha 15} \\ V_{s\beta 41} & V_{s\beta 9} & V_{s\beta 11} & V_{s\beta 15} \\ V_{sx 41} & V_{sx 9} & V_{sx 11} & V_{sx 15} \\ V_{sy 41} & V_{sy 9} & V_{sy 11} & V_{sy 15} \end{bmatrix}^{-1} \begin{bmatrix} v_{s\alpha}^* T_s \\ v_{s\beta}^* T_s \\ v_{sx}^* T_s \\ v_{sy}^* T_s \end{bmatrix} \\ t_0 &= T_s - (t_1 + t_2 + t_3 + t_4). \end{aligned} \quad (\text{A7})$$

485 Substituting (A6) in (A7), the applying times can be calcu-  
486 lated as follows:

$$\begin{aligned} \begin{bmatrix} t_1 \\ t_2 \\ t_3 \\ t_4 \end{bmatrix} &= \frac{T_s}{2V_{dc}} \begin{bmatrix} 1 & -\sqrt{3} & -1 & -\sqrt{3} \\ \sqrt{3}-1 & \sqrt{3}-1 & \sqrt{3}+1 & \sqrt{3}+1 \\ 0 & 2 & 0 & v-2 \\ -(\sqrt{3}-2) & -1 & -(\sqrt{3}+2) & 1 \end{bmatrix} \begin{bmatrix} v_{s\alpha}^* \\ v_{s\beta}^* \\ v_{sx}^* \\ v_{sy}^* \end{bmatrix}. \end{aligned} \quad (\text{A8})$$

487 With  $v_{sx}^* = v_{sy}^* = 0$ , (A8) can be written as:

$$\begin{aligned} \begin{bmatrix} t_1 \\ t_2 \\ t_3 \\ t_4 \end{bmatrix} &= \frac{T_s}{2V_{dc}} \begin{bmatrix} 1 & -\sqrt{3} \\ \sqrt{3}-1 & \sqrt{3}-1 \\ 0 & 2 \\ -(\sqrt{3}-2) & -1 \end{bmatrix} \begin{bmatrix} v_{s\alpha}^* \\ v_{s\beta}^* \end{bmatrix} = \begin{bmatrix} T_2 \\ T_5 \\ T_4 \\ -T_1 \end{bmatrix}. \end{aligned} \quad (\text{A9})$$

#### 488 APPENDIX B 489 MAXIMUM MODULATION INDEX CALCULATION

490 The maximum modulation index  $m_{\max}$  can be obtained  
491 by solving  $t_0 = T_s - (t_1 + t_2 + t_3 + t_4) = 0$ . For example in  
492 sector 1, the sum of the applying times of the active voltage  
493 vectors is calculated from (A9) as:

$$\theta \in \left[0, \frac{\pi}{12}\right] \quad t_1 + t_2 + t_3 + t_4 = \frac{T_s}{V_{dc}} v_{s\alpha}^* \quad (\text{B1})$$

494 where  $v_{s\alpha}^* = \sqrt{3}V_{1m} \cos(\theta)$ ,  $v_{s\beta}^* = \sqrt{3}V_{1m} \sin(\theta)$

$$V_{1m} = mV_{1m6step} = m2V_{dc}/\pi.$$

When

$$t_0 = 0 : T_s = t_1 + t_2 + t_3 + t_4 = 2\sqrt{3}\frac{T_s}{\pi}m \cos(\theta) \quad (\text{B2})$$

From (B2), the modulation index equation can be given as: 496

$$m = \frac{\pi}{2\sqrt{3} \cos(\theta)}. \quad (\text{B3})$$

To determine the angle  $\theta$  corresponding to  $m_{\max}$ , (B3) is 497  
derived: 498

$$\frac{dm}{d\theta} = \frac{\pi \sin(\theta)}{2\sqrt{3} \cos^2(\theta)}. \quad (\text{B4})$$

Equation (B4) is solved for  $\theta = 0$ . Thus, replacing  $\theta$  in (B3): 499

$$m_{\max} = \frac{\pi}{2\sqrt{3} \cos(0)} = \frac{\pi}{2\sqrt{3}} \approx 0.907. \quad (\text{B5})$$

#### APPENDIX C 500 ANALYTICAL FORMULAS OF THE RMS HARMONIC FLUX 501

The per-fundamental cycle rms normalized harmonic flux 502  
 $\tilde{\lambda}_{sfrms}$  was calculated for all the discussed PWM techniques. 503  
Only the analytical formulas of the proposed 24-sector PWMs 504  
are presented here and the ones of the 12-sector PWMs can be 505  
found in [10]. These formulas are given below. 506

##### A. Continuous Modulation C6 $\phi$ SVPWM24 507

$$\begin{aligned} \tilde{\lambda}_{s\alpha\beta frms}^2(m) &= \frac{1}{48}m^2 + \frac{1}{144\pi^2} \\ &\quad \times (56\sqrt{3} + 63\sqrt{6} - 57\sqrt{2} - 228)m^3 \\ &\quad + \frac{1}{32\pi^3}(24\pi + 27 - 21\sqrt{3} - 8\sqrt{3}\pi)m^4 \\ \tilde{\lambda}_{sxy frms}^2(m) &= \frac{1}{144\pi^2}(63\sqrt{6} + 18 - 52\sqrt{3} - 57\sqrt{2})m^3. \end{aligned} \quad (\text{C1})$$

##### B. Discontinuous Modulation D6 $\phi$ SVPWM24-B1 508

$$\begin{aligned} \tilde{\lambda}_{s\alpha\beta frms}^2(m) &= \frac{25}{432}m^2 - \frac{25}{5184\pi^2} \\ &\quad \times (633\sqrt{2} + 408 - 56\sqrt{3} - 387\sqrt{6})m^3 \\ &\quad - \frac{25}{576\pi^3}(15\sqrt{3} + 8\sqrt{3}\pi - 24\pi - 45)m^4 \\ \tilde{\lambda}_{sxy frms}^2(m) &= \frac{25}{5184\pi^2}(63\sqrt{6} + 18 - 52\sqrt{3} - 57\sqrt{2})m^3. \end{aligned} \quad (\text{C2})$$

##### C. Discontinuous Modulation D6 $\phi$ SVPWM24-B2 509

$$\begin{aligned} \tilde{\lambda}_{s\alpha\beta frms}^2(m) &= \frac{1}{27}m^2 - \frac{1}{324\pi^2} \\ &\quad \times (129\sqrt{2} + 45\sqrt{6} + 48 - 56\sqrt{3})m^3 \\ &\quad + \frac{1}{6\pi^3}(2\pi + 3 - \sqrt{3})m^4 \\ \tilde{\lambda}_{sxy frms}^2(m) &= \frac{1}{324\pi^2}(63\sqrt{6} + 18 - 52\sqrt{3} - 57\sqrt{2})m^3. \end{aligned} \quad (\text{C3})$$

510

## REFERENCES

- 511 [1] V. T. Somasekhar, K. Gopakumar, M. R. Baiju, K. K. Mohapatra, and  
512 L. Umanand, "A multilevel inverter system for an induction motor with  
513 open-end windings," *IEEE Trans. Ind. Electron.*, vol. 52, no. 3, pp. 824–  
514 836, Jun. 2005.
- 515 [2] R. C. Portillo *et al.*, "Modeling strategy for back-to-back three-level con-  
516 verters applied to high-power wind turbines," *IEEE Trans. Ind. Electron.*,  
517 vol. 53, no. 5, pp. 1483–1491, Oct. 2006.
- 518 [3] A. K. Gupta and A. M. Khambadkone, "A space vector PWM scheme for  
519 multilevel inverters based on two-level space vector PWM," *IEEE Trans.*  
520 *Ind. Electron.*, vol. 53, no. 5, pp. 1631–1639, Oct. 2006.
- 521 [4] K. Hatua and V. T. Ranganathan, "Direct torque control schemes for  
522 split-phase induction machine," *IEEE Trans. Ind. Appl.*, vol. 41, no. 5,  
523 pp. 1243–1254, Sep./Oct. 2005.
- 524 [5] Y. Zhao and T. A. Lipo, "Space vector PWM control of dual three-phase  
525 induction machine using vector space decomposition," *IEEE Trans. Ind.*  
526 *Appl.*, vol. 31, no. 5, pp. 1100–1109, Sep./Oct. 1995.
- 527 [6] M. A. Abbas, R. Christen, and T. M. Jahns, "Six-phase voltage source  
528 inverter driven induction motor," *IEEE Trans. Ind. Appl.*, vol. IA-20, no. 5,  
529 pp. 1251–1259, Sep./Oct. 1984.
- 530 [7] D. Hadiouche, H. Razik, and A. Rezzoug, "On the modeling and design  
531 of dual-stator windings to minimize circulating harmonic currents for VSI  
532 fed AC machines," *IEEE Trans. Ind. Appl.*, vol. 40, no. 2, pp. 506–515,  
533 Mar./Apr. 2004.
- 534 [8] A. R. Muñoz and T. A. Lipo, "Dual stator winding induction machine  
535 drive," *IEEE Trans. Ind. Appl.*, vol. 36, no. 5, pp. 1369–1379,  
536 Sep./Oct. 2000.
- 537 [9] K. Gopakumar, V. T. Ranganathan, and S. R. Bhat, "Split-phase induction  
538 motor operation from PWM voltage source inverter," *IEEE Trans. Ind.*  
539 *Appl.*, vol. 29, no. 5, pp. 927–932, Sep./Oct. 1993.
- 540 [10] D. Hadiouche, L. Baghli, and A. Rezzoug, "Space vector PWM  
541 techniques for dual three-phase AC machine: Analysis, performance  
542 evaluation, and DSP implementation," *IEEE Trans. Ind. Appl.*, vol. 42,  
543 no. 4, pp. 1112–1122, Jul./Aug. 2006.
- 544 [11] R. Bojoi, M. Lazzari, F. Profumo, and A. Tenconi, "Digital field-oriented  
545 control for dual three-phase induction motor drives," *IEEE Trans. Ind.*  
546 *Appl.*, vol. 39, no. 3, pp. 752–760, May/Jun. 2003.
- 547 [12] K. K. Mohapatra, R. S. Kanchan, M. R. Baiju, P. N. Tekwani, and  
548 K. Gopakumar, "Independent field-oriented control of two split-phase  
549 induction motors from a single six-phase inverter," *IEEE Trans. Ind.*  
550 *Electron.*, vol. 52, no. 5, pp. 1372–1382, Oct. 2005.
- 551 [13] W. Tiejun, G. Chenglin, C. Yongbing, and J. Xiaoyi, "Research on har-  
552 monics of multiphase induction motors," in *Proc. IEEE IEMDC*, Antalya,  
553 Turkey, May 3–5, 2007, pp. 1524–1528.
- 554 [14] J. W. Kolar, H. Ertl, and F. C. Zach, "Influence of the modulation method  
555 on the conduction and switching losses of a PWM converter system,"  
556 *IEEE Trans. Ind. Appl.*, vol. 27, no. 6, pp. 1063–1075, Nov./Dec. 1991.
- 557 [15] K. Marouani, L. Baghli, D. Hadiouche, A. Kheloui, and A. Rezzoug,  
558 "Discontinuous SVPWM techniques for double star induction motor  
559 drive control," in *Proc. IEEE IECON*, Paris, France, Nov. 6–10, 2006,  
560 pp. 902–907.
- 561 [16] G. K. Singh, K. Nam, and S. K. Lim, "A simple indirect field-oriented  
562 control scheme for multiphase induction machine," *IEEE Trans. Ind.*  
563 *Electron.*, vol. 52, no. 4, pp. 1177–1184, Aug. 2005.
- 564 [17] D. C. Lee and G. M. Lee, "Linear control of inverter output voltage in  
565 overmodulation," *IEEE Trans. Ind. Electron.*, vol. 44, no. 4, pp. 590–592,  
566 Aug. 1997.
- 567 [18] S. R. Bowes and Y. S. Lai, "The relationship between space-vector mod-  
568 ulation and regular-sampled PWM," *IEEE Trans. Ind. Electron.*, vol. 44,  
569 no. 5, pp. 670–679, Oct. 1997.
- 570 [19] O. Ojo, "The generalized discontinuous PWM scheme for three-phase  
571 voltage source inverters," *IEEE Trans. Ind. Electron.*, vol. 51, no. 6,  
572 pp. 1280–1289, Dec. 2004.
- 573 [20] A. M. Hava, R. J. Kerkman, and T. A. Lipo, "Simple analytical and graph-  
574 ical methods for carrier-based PWM-VSI drives," *IEEE Trans. Power*  
575 *Electron.*, vol. 14, no. 1, pp. 49–61, Jan. 1999.
- 576 [21] S. Ogasawara, H. Akagi, and A. Nabae, "A novel PWM scheme of voltage  
577 source inverters based on space vector theory," in *Proc. EPE*, Aachen,  
578 Germany, Oct. 1989, pp. 1197–1202.
- 579 [22] H. W. van der Broeck, H. C. Skudelyni, and G. V. Stanke, "Analysis and  
580 realization of a pulsewidth modulator based on voltage space vectors,"  
581 *IEEE Trans. Ind. Appl.*, vol. 24, no. 1, pp. 142–150, Jan./Feb. 1988.
- 582 [23] J. Holtz and B. Beyer, "Optimal pulse width modulation for AC servos  
583 and low-cost industrial drives," *IEEE Trans. Ind. Appl.*, vol. 30, no. 4,  
584 pp. 1039–1047, Jul./Aug. 1994.
- 585 [24] *TMS320F/C240 DSP Controllers Reference Guide, Peripheral and Spe-*  
586 *cific Devices*, Texas Instruments, Dallas, TX, 1999. Literature Number  
587 SPRU161C.



**Khoudir Marouani** was born in 1972. He received 588 **AQ1**  
the Degree of Engineer in automatics and the Degree 589  
of Magister in electrical engineering from the Poly- 590  
technic Military School (EMP), Algiers, Algeria, in 591  
1996 and 2000, respectively, where he is currently 592  
working toward the Ph.D. degree in the Electrical 593  
Engineering Laboratory. 594

He is currently working as a Research and Teach- 595  
ing Assistant with the Electrical Engineering Lab- 596  
oratory, EMP. His research interests include power 597  
electronics, electrical drives and active power filters. 598



**Lotfi Baghli** was born in 1971. He received the 599 **AQ2**  
Electrical Engineering Diploma degree (with honors) 600  
from the Ecole Nationale Polytechnique, Algiers, 601  
Algeria, in 1989, and the DEA degree in electri- 602  
cal engineering from the Université Henri Poincaré, 603  
Nancy, France, in 1995 and 1999, respectively. 604

He is currently a Lecturer at IUFM de Lorraine 605 **AQ3**  
and a member of Groupe de Recherche en Elec- 606  
trotechnique et Electronique de Nancy, Nancy. His 607  
works concern digital control using DSP, PSO and 608  
genetic algorithms applied to the control and identi- 609  
fication of electrical machines. 610



**Djafar Hadiouche** was born in 1974. He received 611 **AQ4**  
the Ph.D. degree in electrical engineering from the 612  
University Henri Poincaré, Nancy, France, in 2001. 613

Until 2002, he was Assistant Lecturer in the 614  
same university and did research in the laboratory 615  
of the "Groupe de Recherche en Electrotechnique 616  
et Electronique de Nancy," Nancy. Since 2003, he 617  
has been a Motion Specialist Engineer with GE 618  
Fanuc Automation Solutions Europe, Echternach, 619  
Luxembourg. His main tasks include servosizing, 620  
tools and motion programs development, electronic 621  
cam profiling and motion technical training. His main research interests concern 622  
multiphase ac machines, their modeling, identification, pulsewidth modulation 623  
techniques, and vector control. 624

Dr. Hadiouche received the Best Prize Paper Award from the Electric 625  
Machine Committee at the 2001 IEEE IAS Annual Meeting. 626



**Abdelaziz Kheloui** was born in 1969. He received 627 **AQ5**  
the M.Sc.Eng. degree from the Ecole Nationale 628  
d'ingénieurs et Techniciens d'Algérie, Algiers, 629  
Algeria, in 1990, and the Ph.D. degree in electrical 630  
engineering from the Institut National Polytechnique 631  
de Lorraine, Nancy, France, in 1994. 632

Since 1994, he has been a Researcher and a 633  
Teacher at the electrical engineering laboratory of 634  
the Polytechnic Military School, Algiers, Algeria. 635  
His current research interests are control of electrical 636  
drives and power electronics. 637



**Abderrezak Rezzoug** was born in 1948. He received 638 **AQ6**  
the Electrical Engineer degree, Dr. Ing. diploma, 639  
and Ph.D. degree from ENSEM Institut National 640 **AQ7**  
Polytechnique de Lorraine, Nancy, France, in 1972, 641  
1979, and 1987, respectively. 642

He is currently a Professor in electrical engineer- 643  
ing at the Université Henri Poincaré, Nancy. As a 644  
member of the Groupe de Recherche en Electrotech- 645  
nique et Electronique de Nancy, Nancy, his main 646  
areas of research concern electrical machines, their 647  
identification, diagnostic and control, and supercon- 648  
ducting applications. 649

## AUTHOR QUERIES

AUTHOR PLEASE ANSWER ALL QUERIES

AQ1 = “1972” was assumed as the author’s birth year. Please check if appropriate.

AQ2 = “1971” was assumed as the author’s birth year. Please check if appropriate.

AQ3 = Please provide the expanded form of the acronym “IUFM”.

AQ4 = “1974” was assumed as the author’s birth year. Please check if appropriate.

AQ5 = “1969” was assumed as the author’s birth year. Please check if appropriate.

AQ6 = “1948” was assumed as the author’s birth year. Please check if appropriate.

AQ7 = Please provide the expanded form of the acronym “ENSEM”.

Note: Figure citations were renumbered. The original sequence was 1-2-3-4-5-6-7-9-8.

END OF ALL QUERIES

LEEE  
PROOF

# A New PWM Strategy Based on a 24-Sector Vector Space Decomposition for a Six-Phase VSI-Fed Dual Stator Induction Motor

Khoudir Marouani, Lotfi Baghli, Djafar Hadiouche, Abdelaziz Kheloui, and Abderrezak Rezzoug

**Abstract**—This paper presents a new space vector pulsewidth modulation (SVPWM) technique for the control of six-phase voltage source inverter (VSI)-fed dual stator induction machines (DSIM). A DSIM is an induction machine which has two sets of three-phase stator windings spatially shifted by 30 electrical degrees and fed by two three-phase VSIs. Despite their advantage of power segmentation, these machines are characterized by large zero sequence harmonic currents, and in particular those of order  $6k \pm 1$ , which are due to the mutual cancellation between the two stator windings. The proposed SVPWM scheme, while easy to implement digitally, reduces significantly these extra stator harmonic currents. Experimental results, collected from a 15 kW prototype machine controlled by a digital signal processor are presented and discussed.

**Index Terms**—Dual stator induction machines (DSIM), six-phase voltage source inverter (VSI), space vector pulsewidth modulation (SVPWM).

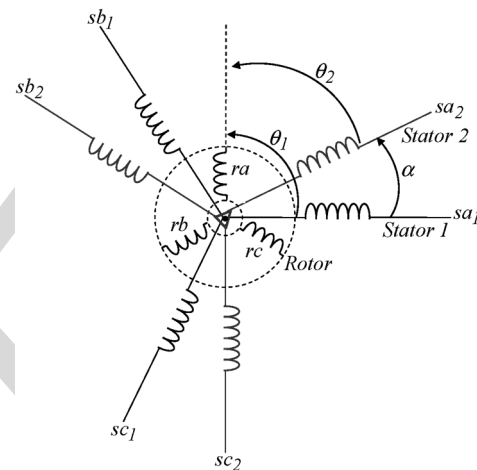


Fig. 1. DSIM windings.

## I. INTRODUCTION

NOWADAYS, electrical machine drives are widely used in industrial applications and transportation systems such as electric/hybrid vehicles, traction locomotives and electric propulsion ships, where high-power levels in conjunction with high-performance requirements are more and more demanded. To achieve these high ratings, there are two possible approaches; one focuses on the converter side by increasing the number of output voltage levels and the other one on the machine side by increasing the number of phases. In the first approach, the idea is to divide the high dc bus voltage into multiple low levels and therefore to distribute the high power required among cells of reduced-voltage power switches without the problem of dynamic voltage sharing encountered in the series connection of active devices. However, increasing the number of inverter levels adds to the control complexity and may introduce some voltage imbalance problems [1]–[3]. It is a solution well suited for high-power and high-voltage utility ap-

plications. For adjustable speed drives, however, an alternative approach is to use a multiphase machine, i.e., a machine with more than three phases in the stator, since the number of phases is not imposed anyway, given that the machine is connected to the electric supply through a dc/ac converter. The number of phases could be used instead as an additional degree of freedom in the overall system design [4].

Although the answer to the question whether it is better to use a multilevel inverter-fed three-phase machine or a multiphase machine depends on the application, it is undeniable that the latter option offers several advantages which may make it appear very attractive. In fact, the most significant features are a low torque ripple, a reduction in the power per phase and fault-tolerance capability. Other interesting advantages can be pointed out, such as a better torque production per ampere for the same machine volume, higher efficiency and improved reliability [5], [6].

A common type of multiphase machine is the dual stator induction machine (DSIM), where two sets of three-phase windings, spatially phase shifted by 30 electrical degrees, share a common stator magnetic core as shown in Fig. 1.

Due to the development of fast switching power semiconductor devices, voltage source inverters (VSIs) are preferred in variable speed machine drives. As VSI-fed multiphase machines are gaining increasing interest for high-power applications, various pulsewidth modulation (PWM) techniques have been developed accordingly, as they strongly affect the overall inverter efficiency and output voltage waveform quality.

Manuscript received February 28, 2007; revised September 24, 2007.

K. Marouani and A. Kheloui are with the Electrical Engineering Laboratory, Polytechnic Military School, 16111 Algiers, Algeria (e-mail: marouani\_khoudir@yahoo.fr; akheloui@caramail.com).

L. Baghli and A. Rezzoug are with the Groupe de Recherche en Electrotechnique et Electronique de Nancy, CNRS UMR 7037, Université Henri Poincaré, 54506 Nancy Cedex, France (e-mail: lotfi.baghli@green.uhp-nancy.fr; abderrezak.rezzoug@green.uhp-nancy.fr).

D. Hadiouche is with the GE Fanuc Automation Solutions Europe, 6468 Echternach, Luxembourg (e-mail: djafar.hadiouche@wanadoo.fr).

Color versions of one or more of the figures in this paper are available online at <http://ieeexplore.ieee.org>.

Digital Object Identifier 10.1109/TIE.2008.918486

68 In a VSI-fed DSIM, the two stator windings are mutually  
69 coupled and small unbalances in the two supply voltages may  
70 generate high currents [7]. Furthermore, because of the low  
71 impedance seen by the voltage harmonic components generated  
72 by the switched voltage waveforms, harmonic currents of high  
73 level are circulating uselessly in the two stator windings, adding  
74 to the overall losses and therefore to the semiconductor devices  
75 ratings [8], [9].

76 To minimize these extra harmonic currents in a six-phase  
77 VSI-fed DSIM, a new 24-sector PWM technique is proposed  
78 in this paper and tested on a 15 kW laboratory machine. The  
79 digital implementation is carried out on a DS1104 dSPACE  
80 controller board. A comparative study between the proposed  
81 technique and similar space vector PWM (SVPWM) techniques  
82 [5], [10], based on analytical harmonic current analysis, is also  
83 developed and discussed.

84

## II. MACHINE MODEL

85 The machine model is based on the assumption that space  
86 harmonics and magnetic saturation are negligible, and that the  
87 two stator three-phase windings are identical and symmetrical  
88 with the two neutrals being isolated. In order to derive a prac-  
89 tical model suitable for control, a decoupling transformation  
90 matrix is used, as proposed in [5]–[7]. The matrix has the  
91 following form:

$$[T_S]^{-1} = \frac{1}{\sqrt{3}} \begin{bmatrix} 1 & -\frac{1}{2} & -\frac{1}{2} & \frac{\sqrt{3}}{2} & -\frac{\sqrt{3}}{2} & 0 \\ 0 & \frac{\sqrt{3}}{2} & -\frac{\sqrt{3}}{2} & \frac{1}{2} & \frac{1}{2} & -1 \\ \hline 1 & -\frac{1}{2} & -\frac{1}{2} & -\frac{\sqrt{3}}{2} & \frac{\sqrt{3}}{2} & 0 \\ 0 & -\frac{\sqrt{3}}{2} & \frac{\sqrt{3}}{2} & \frac{1}{2} & \frac{1}{2} & -1 \\ \hline 1 & 1 & 1 & 0 & 0 & 0 \\ 0 & 0 & 0 & 1 & 1 & 1 \end{bmatrix}. \quad (1)$$

92 By applying (1) to the voltage vector equations, the overall  
93 machine model is transformed into three decoupled submodels,  
94 written in three independent space coordinates, identified as  
95  $(\alpha-\beta)$ ,  $(x-y)$ , and  $(o_1-o_2)$ , respectively.

96 The machine voltage submodel in  $(\alpha-\beta)$  coordinates can be  
97 written as:

$$\begin{bmatrix} v_{s\alpha} \\ v_{s\beta} \\ v_{r\alpha} \\ v_{r\beta} \end{bmatrix} = \begin{bmatrix} R_s & 0 & 0 & 0 \\ 0 & R_s & 0 & 0 \\ 0 & M\dot{\theta} & R_r & L_r\dot{\theta} \\ -M\dot{\theta} & 0 & -L_r\dot{\theta} & R_r \end{bmatrix} \begin{bmatrix} i_{s\alpha} \\ i_{s\beta} \\ i_{r\alpha} \\ i_{r\beta} \end{bmatrix} + \begin{bmatrix} L_s & 0 & M & 0 \\ 0 & L_s & 0 & M \\ M & 0 & L_r & 0 \\ 0 & M & 0 & L_r \end{bmatrix} \frac{d}{dt} \begin{bmatrix} i_{s\alpha} \\ i_{s\beta} \\ i_{r\alpha} \\ i_{r\beta} \end{bmatrix} \quad (2)$$

98 where  $\dot{\theta} = \Omega_m$  is the rotor mechanical speed, and  $L_s = L_{ls} +$   
99  $3L_{ms}$ ,  $L_r = L_{lr} + (3/2)L_{mr}$ ,  $M = (3/\sqrt{2})M_{sr}$ .  $L_{ls}$  and  $L_{lr}$   
100 are the stator and rotor leakage inductances in  $(\alpha-\beta)$  coordi-  
101 nates, respectively.

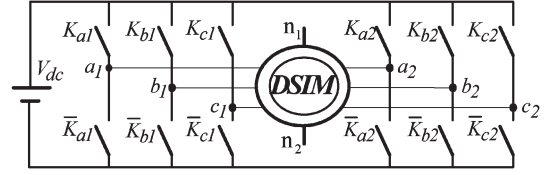


Fig. 2. Six-phase VSI fed DSIM.

102 The DSIM  $(\alpha-\beta)$  submodel expressed in the stationary  
103 reference frame is similar to the three-phase induction machine  
104 model [11].

105 The machine voltage submodel in  $(x-y)$  coordinates is  
106 given by:

$$\begin{bmatrix} v_{sx} \\ v_{sy} \end{bmatrix} = \begin{bmatrix} R_s & 0 \\ 0 & R_s \end{bmatrix} \begin{bmatrix} i_{sx} \\ i_{sy} \end{bmatrix} + \begin{bmatrix} L_{lsxy} & 0 \\ 0 & L_{lsxy} \end{bmatrix} \frac{d}{dt} \begin{bmatrix} i_{sx} \\ i_{sy} \end{bmatrix} \quad (3)$$

107 where  $L_{lsxy}$  is the transformed stator leakage inductance in  
108  $(x-y)$  coordinates.

109 The machine voltage submodel in  $(o_1-o_2)$  coordinates is  
110 expressed as follows:

$$\begin{bmatrix} v_{so1} \\ v_{so2} \\ v_{ro} \end{bmatrix} = \begin{bmatrix} R_s & 0 & 0 \\ 0 & R_s & 0 \\ 0 & 0 & R_r \end{bmatrix} \begin{bmatrix} i_{so1} \\ i_{so2} \\ i_{ro} \end{bmatrix} + \begin{bmatrix} L_{lso} & 0 & 0 \\ 0 & L_{lso} & 0 \\ 0 & 0 & L_{lr} \end{bmatrix} \frac{d}{dt} \begin{bmatrix} i_{so1} \\ i_{so2} \\ i_{ro} \end{bmatrix} \quad (4)$$

111 where  $L_{lso}$  is the transformed stator leakage inductance in  
112  $(o_1-o_2)$  coordinates.

113 The electromagnetic torque of the DSIM is expressed only  
114 in terms of stator and rotor  $(\alpha-\beta)$  current components, since  
115 the  $(x-y)$  and  $(o_1-o_2)$  counterparts do not contribute to the  
116 electromechanical energy conversion, as shown by (3) and (4).  
117 The expression of the electromagnetic torque is then as follows:

$$T_e = pM(i_{s\beta}i_{r\alpha} - i_{s\alpha}i_{r\beta}) \quad (5)$$

118 where  $p$  is the number of pole pairs.

### General Remarks

119  
120 The  $(x-y)$  and  $(o_1-o_2)$  current components do not con-  
121 tribute to the air-gap flux linkages. Hence, they are limited only  
122 by the stator resistance and leakage inductance [12], [13]. They  
123 produce only losses and therefore must be kept equal to zero or  
124 as small as possible.

125 The transformed voltage equations in the three subframes  
126 are well decoupled and, as a result, both machine analysis and  
127 control are greatly simplified.

## III. SVPWM CONTROL OF A DOUBLE-STAR INDUCTION MOTOR

128  
129  
130 The drive system is a six-phase VSI fed DSIM, as shown  
131 in Fig. 2. A combinatorial analysis of the inverter switch  
132 states shows 64 switching modes. Thus, 64 different voltage  
133 vectors can be applied to the machine. Each voltage vector is  
134 represented by a decimal number corresponding to the binary  
135 number  $(K_{c2}K_{b2}K_{a2}K_{c1}K_{b1}K_{a1})$ , which gives the state of

136 the upper switches. By using the  $(6 \times 6)$  transformation matrix  
 137  $[Ts]^{-1}$ , each voltage vector can be decomposed into  $(\alpha-\beta)$ ,  
 138  $(x-y)$ , and  $(o_1-o_2)$  voltages. The  $(o_1-o_2)$  ones are all equal  
 139 to zero because the neutrals  $(n_1, n_2)$  of the two winding sets  
 140 are isolated. So the SVPWM strategy operates in two complex  
 141 planes  $(\alpha-\beta)$  and  $(x-y)$ . Four variables need to be controlled  
 142 simultaneously during each sampling period, by generating  
 143 maximum  $(\alpha-\beta)$  and minimum  $(x-y)$  voltage amplitudes.  
 144 Therefore, during each sampling period, a set of four active  
 145 voltage vectors must be chosen to fulfil these two conditions,  
 146 according to the reference voltage vector location. There are  
 147 numerous ways for choosing such a set.

148 A. Six-Phase SVPWM Techniques

149 The principle of the PWM control techniques proposed in  
 150 [5] and [10] is to choose switching sequences in such a way  
 151 that two consecutive nonzero voltage vectors are practically  
 152 opposite in phase in the  $(x-y)$  plane. In this way, each change  
 153 in the applied vectors leads to a sequence of increases and  
 154 decreases in  $(x-y)$  currents around zero. Moreover, in order  
 155 to minimize  $(x-y)$  harmonic currents and maintain the lowest  
 156 switching frequency, there are different choices to allocate  
 157 zero voltage vectors (0, 7, 56 or 63) within the switching  
 158 sequences. Thus, the switching sequences presented in [10] lead  
 159 to continuous and discontinuous modulation techniques and,  
 160 consequently, to different harmonic distortion characteristics.  
 161 A modulation technique is continuous when on/off switching  
 162 occurs within every sampling period, for all inverter legs and  
 163 all sectors. A modulation technique is discontinuous when one  
 164 (or more) inverter leg stops switching, i.e., the corresponding  
 165 phase voltage is clamped to the positive or negative dc bus for  
 166 at least one sector [14].

167 B. 12-Sector SVPWM Technique

168 In the SVPWM technique addressed in [5], only the  $(\alpha-\beta)$   
 169 voltage vectors having maximum magnitude (45, 41, 9, 11,  
 170 27, 26, 18, 22, 54, 52, 36, 37) are employed to synthesize  
 171 the reference voltage vector  $v_{s\alpha\beta}^*$ . These voltage vectors divide  
 172 the  $(\alpha-\beta)$  plane into 12 sectors and each sector is  $\pi/6$  rad,  
 173 as shown in Fig. 3. For example, voltage vectors 45, 41, 9,  
 174 and 11 are selected when the reference voltage vector is located  
 175 in sector 1. As shown in Fig. 4, continuous and discontinuous  
 176 modulation techniques can be obtained according to the switch-  
 177 ing sequences given below.

178 1) Continuous Modulation C6  $\phi$  SVPWM12: For example,  
 179 when the reference voltage vector is located in sector 1, a con-  
 180 tinuous modulation technique (C6  $\phi$  SVPWM12) is obtained  
 181 with the following sequence:

$$|7-45-41-56-9-11-7|7-11-9-56-41-45-7|.$$

182 2) Discontinuous Modulation D6  $\phi$  SVPWM12-A: For the  
 183 same sector 1, a discontinuous modulation technique (D6  $\phi$   
 184 SVPWM12-A) can be obtained with the following sequence:

$$|7-45-41-9-11-7|7-11-9-41-45-7|.$$

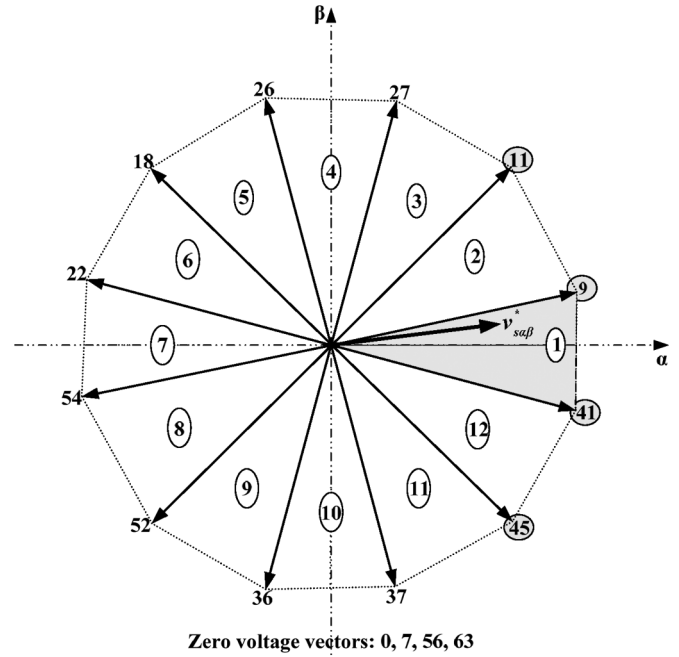


Fig. 3. Presentation of the inverter voltage vectors having maximum magnitude in  $(\alpha-\beta)$  plane.

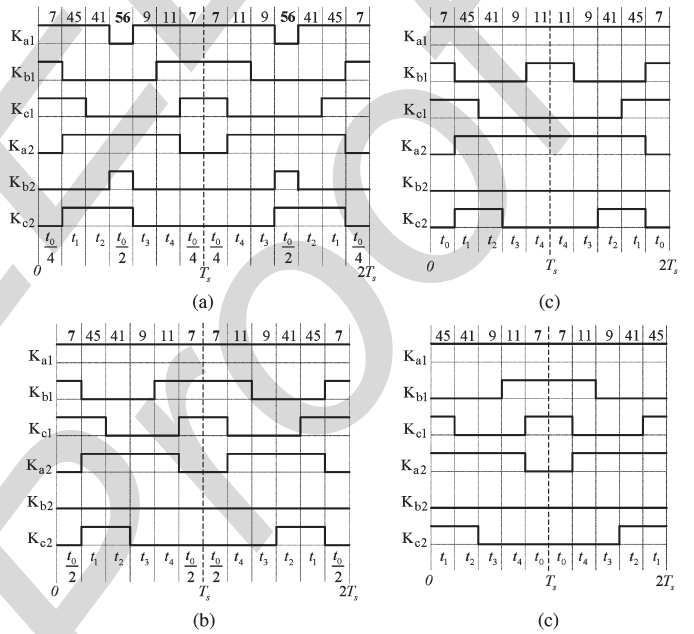


Fig. 4. Twelve-sector SVPWM switching sequences when the reference voltage vector is located in sector 1. (a) C6  $\phi$  SVPWM12. (b) D6  $\phi$  SVPWM12-A. (c) D6  $\phi$  SVPWM12-B1. (d) D6  $\phi$  SVPWM12-B2.

3) Discontinuous Modulation D6  $\phi$  SVPWM12-B1: In the 185  
 D6  $\phi$  SVPWM12-B1, the zero-voltage vectors are applied at the 186  
 beginning and at the end of the switching sequence as follows: 187

$$|7-45-41-9-11|11-9-41-45-7|.$$

4) Discontinuous Modulation D6  $\phi$  SVPWM12-B2: In the 188  
 D6  $\phi$  SVPWM12-B2, the zero-voltage vectors are applied in 189  
 the middle of the switching sequence as follows: 190

$$|45-41-9-11-7|7-11-9-41-45|.$$

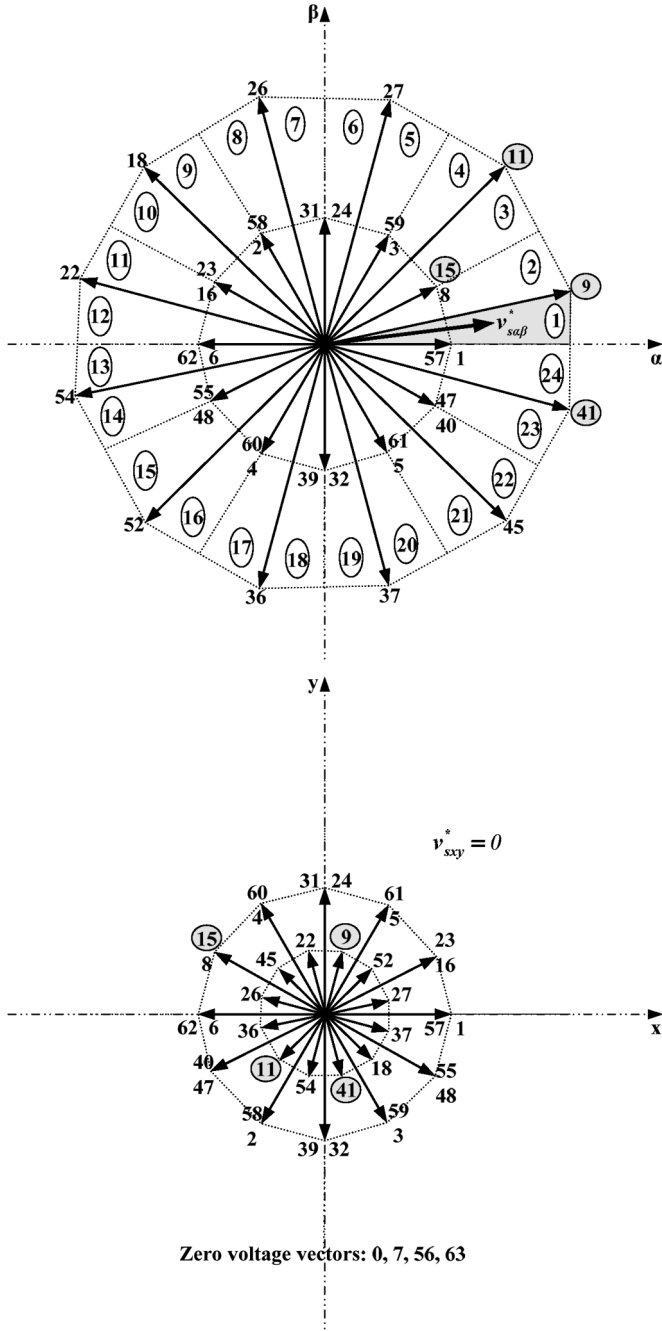


Fig. 5. Presentation of the inverter voltage vectors having maximum and half magnitude in  $(\alpha-\beta)$ , and  $(x-y)$  planes.

### 191 C. Proposed 24-Sector SVPWM Technique

192 As shown in Fig. 4, the switching pattern corresponding  
193 to the switching sequences of the 12-sector PWM techniques  
194 presents asymmetrical waveforms and usually more than two  
195 transitions (from low to high or from high to low) occur on  
196 the corresponding PWM outputs within a sampling period,  
197 which increases the switching frequency of the inverter legs  
198 and causes difficulties for digital signal processor (DSP) im-  
199 plementation of these strategies. Accordingly, some additional  
200 adaptations in DSP programs are necessary to ensure successful  
201 experiments [15], [16].

202 To overcome these drawbacks, the new 24-sector SVPWM  
203 technique proposed in this paper combines the maximum

magnitude  $(\alpha-\beta)$  voltage vectors and the ones with half  
204 magnitude (1, 57, 8, 15, 3, 59, 24, 31, 2, 58, 16, 23, 6, 205  
62, 48, 55, 4, 60, 32, 39, 5, 61, 40, 47) generated by one 206  
inverter. These voltage vectors divide the  $(\alpha-\beta)$  plane into 207  
twenty four  $\pi/12$ -rad sectors, as shown in Fig. 5. In each 208  
sampling period, the reference voltage vector is achieved by 209  
selecting a set of three voltage vectors among those having 210  
maximum magnitude and a fourth vector among the ones with 211  
half magnitude. For example, voltage vectors 41, 9, 11 and 15 212  
are selected when the reference voltage vector is located in 213  
sector 1. Then, the voltage vectors applying times:  $t_1, t_2, t_3$  and 214  
 $t_4$  are obtained as explained in Appendix A. For the remaining 215  
time  $t_0 = T_s - (t_1 + t_2 + t_3 + t_4)$ , zero state vectors (0, 7, 56 216  
or 63) are applied. Consequently, simple PWM outputs with 217  
symmetrical waveforms are obtained. As shown in Fig. 6, 218  
only two transitions or less (from low to high or from high 219  
to low) occur on the corresponding PWM outputs within a 220  
sampling period. This fact decreases the switching frequency 221  
of the inverter legs and allows easy DSP implementation. The 222  
switching sequences and the corresponding applying times for 223  
all sectors are presented in Table I. It should also be noticed 224  
that both continuous and discontinuous modulation techniques 225  
can be obtained with this new 24-sector SVPWM scheme. This 226  
is achieved by selecting the appropriate zero voltage vector 227  
locations within the switching sequence. 228

1) *Continuous Modulation C6  $\phi$  SVPWM24*: Continuous 229  
PWM technique (C6  $\phi$  SVPWM24) can be obtained for all sec- 230  
tors by selecting the switching sequences presented in Table I. 231  
As an example, when the reference voltage vector is located 232  
in sector 1, a C6  $\phi$  SVPWM24 is obtained by selecting the 233  
following sequence: 234

$$|56-41-9-11-15-7|7-15-11-9-41-56|.$$

2) *Discontinuous Modulation D6  $\phi$  SVPWM24-B1 and B2*: 235  
Two discontinuous PWM schemes can be obtained through the 236  
appropriate positioning of the zero voltage vectors. In sector 1, 237  
the examples are as follows. 238

1) D6  $\phi$  SVPWM24-B1: The first discontinuous modulation 239  
technique can be obtained by placing the zero voltage 240  
vector both at the beginning and at the end of the switch- 241  
ing sequence, as follows: 242

$$|56-41-9-11-15|15-11-9-41-56|.$$

2) D6  $\phi$  SVPWM24-B2: The second discontinuous mod- 243  
ulation technique is obtained by placing the zero volt- 244  
age vector in the middle of the switching sequence, as 245  
follows: 246

$$|41-9-11-15-7|7-15-11-9-41|.$$

3) *Switching Sequences and Applying Time Selection*: For 247  
optimal DSP implementation and low algorithm execution time, 248  
the applying times ( $t_1, t_2, t_3$ , and  $t_4$ ) computation can be 249  
simplified by an offline calculation for all sectors in the same 250  
manner as for sector 1. As a result, within each sampling period, 251  
there is a total of only 12 coefficients  $T_i$  to be calculated in (6). 252

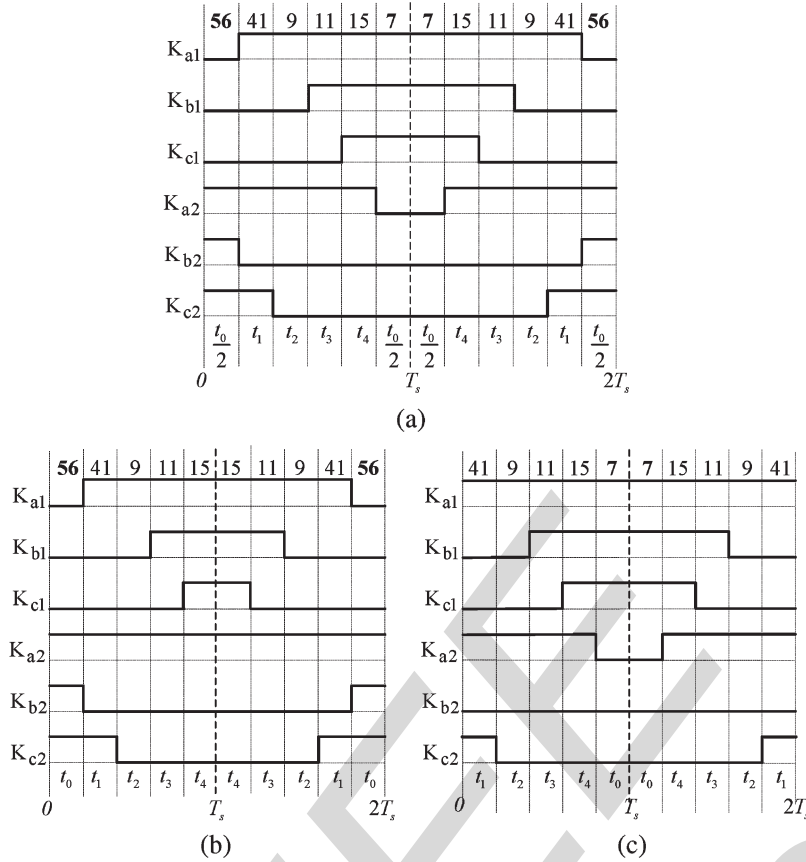


Fig. 6. Twenty-four-sector SVPWM switching sequences when the reference voltage vector is located in sector 1. (a) C6  $\phi$  SVPWM24. (b) D6  $\phi$  SVPWM24-B1. (c) D6  $\phi$  SVPWM24-B2.

253 Table I describes the C6  $\phi$  SVPWM24 switching sequences and  
 254 applying time selection according to the sector number in the  
 255  $(\alpha-\beta)$  plane.

0.907, coincides with the corresponding value for the three- 266  
 phase SVPWM [20]. Note that  $m_{\max}$  is obtained by solving 267  
 $t_0 = T_s - (t_1 + t_2 + t_3 + t_4) = 0$  as shown in Appendix B. 268

$$\begin{bmatrix} T_1 \\ T_2 \\ T_3 \\ T_4 \\ T_5 \\ T_6 \\ T_7 \\ T_8 \\ T_9 \\ T_{10} \\ T_{11} \\ T_{12} \end{bmatrix} = \frac{T_s}{2V_{dc}} \begin{bmatrix} \sqrt{3}-2 & 1 \\ 1 & -\sqrt{3} \\ 1 & \sqrt{3}-2 \\ 0 & 2 \\ \sqrt{3}-1 & \sqrt{3}-1 \\ -(\sqrt{3}-1) & \sqrt{3}-1 \\ \sqrt{3} & -1 \\ 1 & -(\sqrt{3}-2) \\ -(\sqrt{3}-2) & 1 \\ 2 & 0 \\ \sqrt{3} & 1 \\ 1 & \sqrt{3} \end{bmatrix} \begin{bmatrix} v_{s\alpha}^* \\ v_{s\beta}^* \end{bmatrix}. \quad (6)$$

#### 256 D. Maximum Modulation Index

257 The modulation index  $m$  can be defined as the ratio of  
 258 the fundamental component magnitude of the line to neutral  
 259 inverter output voltage  $V_{1m}$  to the fundamental component  
 260 magnitude of the six-step mode voltage  $V_{1m6step} = 2V_{dc}/\pi$   
 261 [17]. When the inverter is operating in the linear modulation  
 262 region, the sum of the applying times of the active voltage  
 263 vectors is less than the switching period  $T_s$  [18], [19]. The  
 264 largest value for linear output with the 12-sector and the  
 265 proposed 24-sector SVPWM techniques,  $m_{\max} = \pi/(2\sqrt{3}) \approx$

#### IV. HARMONIC CURRENT ANALYSIS

269

The voltage and current waveform quality of the PWM-VSI 270  
 drives is determined via the switching frequency harmonics, 271  
 since they determine the switching frequency copper losses 272  
 and the torque ripple of a motor load and the line current 273  
 total harmonic distortion of a line-connected VSI. While the 274  
 copper losses are measured over a fundamental cycle and 275  
 therefore require a per fundamental cycle (macroscopic) rms 276  
 ripple current value calculation, the peak and local stresses 277  
 are properly investigated on a per-carrier cycle (microscopic) 278  
 basis. Therefore, first a microscopic and then a macroscopic 279  
 investigation is required [20]. Because, the machine model 280  
 includes  $(\alpha-\beta)$  and  $(x-y)$  components, the harmonic current 281  
 analysis must be made for the  $(\alpha-\beta)$  and  $(x-y)$  currents. 282

#### A. Normalized Harmonic Currents and Fluxes Calculation

283

The stator voltage equations in the stator coordinate system 284  
 are expressed as follows: 285

$$\begin{aligned} v_{s\alpha\beta} &= R_s i_{s\alpha\beta} + \frac{d\lambda_{s\alpha\beta}}{dt} \\ v_{sxy} &= R_s i_{sxy} + L_{lsxy} \frac{di_{sxy}}{dt} \end{aligned} \quad (7)$$

TABLE I  
PROPOSED C6  $\phi$  SVPWM24 SWITCHING SEQUENCES

Sector	Switching sequences	Voltage vectors applying times			
		$t_1$	$t_2$	$t_3$	$t_4$
1	56-41-9-11-15-7	$T_2$	$T_5$	$T_4$	$-T_1$
2	56-57-41-9-11-7	$T_1$	$T_2$	$T_3$	$T_4$
3	0-9-11-27-59-63	$T_7$	$T_9$	$-T_2$	$-T_6$
4	0-8-9-11-27-63	$T_6$	$T_7$	$T_8$	$-T_2$
5	7-11-27-26-24-56	$T_{10}$	$T_1$	$-T_7$	$T_3$
6	7-3-11-27-26-56	$-T_3$	$T_{10}$	$T_5$	$-T_7$
7	63-27-26-18-2-0	$T_{11}$	$T_6$	$-T_{10}$	$T_8$
8	63-31-27-26-18-0	$-T_8$	$T_{11}$	$T_9$	$-T_{10}$
9	56-26-18-22-23-7	$T_{12}$	$-T_3$	$-T_{11}$	$T_5$
10	56-58-26-18-22-7	$-T_5$	$T_{12}$	$T_1$	$-T_{11}$
11	0-18-22-54-62-63	$T_4$	$-T_8$	$-T_{12}$	$T_9$
12	0-16-18-22-54-63	$-T_9$	$T_4$	$T_6$	$-T_{12}$
13	7-22-54-52-48-56	$-T_2$	$-T_5$	$-T_4$	$T_1$
14	7-6-22-54-52-56	$-T_1$	$-T_2$	$-T_3$	$-T_4$
15	63-54-52-36-4-0	$-T_7$	$-T_9$	$T_2$	$T_6$
16	63-55-54-52-36-0	$-T_6$	$-T_7$	$-T_8$	$T_2$
17	56-52-36-37-39-7	$-T_{10}$	$-T_1$	$T_7$	$-T_3$
18	56-60-52-36-37-7	$T_3$	$-T_{10}$	$-T_5$	$T_7$
19	0-36-37-45-61-63	$-T_{11}$	$-T_6$	$T_{10}$	$-T_8$
20	0-32-36-37-45-63	$T_8$	$-T_{11}$	$-T_9$	$T_{10}$
21	7-37-45-41-40-56	$-T_{12}$	$T_3$	$T_{11}$	$-T_5$
22	7-5-37-45-41-56	$T_5$	$-T_{12}$	$-T_1$	$T_{11}$
23	63-45-41-9-1-0	$-T_4$	$T_8$	$T_{12}$	$-T_9$
24	63-47-45-41-9-0	$T_9$	$-T_4$	$-T_6$	$T_{12}$

286 where the stator and the rotor flux equations are given by:

$$\begin{aligned}\lambda_{s\alpha\beta} &= L_s i_{s\alpha\beta} + M i_{r\alpha\beta} \\ \lambda_{r\alpha\beta} &= L_r i_{r\alpha\beta} + M i_{s\alpha\beta}.\end{aligned}\quad (8)$$

287 The stator flux equation can be rewritten as:

$$\lambda_{s\alpha\beta} = \sigma L_s i_{s\alpha\beta} + \frac{M}{L_r} \lambda_{r\alpha\beta}.\quad (9)$$

288 Substituting (9) in (7), the stator voltage equation can be  
289 expressed as follows:

$$v_{s\alpha\beta} = R_s i_{s\alpha\beta} + \sigma L_s \frac{di_{s\alpha\beta}}{dt} + \frac{M}{L_r} \frac{d\lambda_{r\alpha\beta}}{dt}.\quad (10)$$

290 If only the harmonic voltages and currents are considered,  
291 it will be assumed that the reference voltage vector  $v_{s\alpha\beta}^*$  is  
292 constant over the switching period  $T_s$ , because the switching  
293 frequency  $f_s$  is much higher than the fundamental frequency  
294  $f_e$ , and that the stator and the rotor time constants are much  
295 larger than the switching period, with the resistance drops being  
296 neglected [21]. Under these assumptions, the voltages and

currents can be separated in the harmonic components, which  
change over  $T_s$  while the fundamental components remain  
constant over the same period. Thus, from (7) and (10), the  
harmonic voltage equations can be expressed as follows:

$$\begin{aligned}\tilde{v}_{s\alpha\beta} &= \sigma L_s \frac{d\tilde{i}_{s\alpha\beta}}{dt} \\ \tilde{v}_{sxy} &= L_{lsxy} \frac{d\tilde{i}_{sxy}}{dt}\end{aligned}\quad (11)$$

where  $\tilde{v}_{s\alpha\beta}$  is the harmonic voltage and is equal to the  
difference between the actual voltage vector and the reference  
vector  $v_{s\alpha\beta}^*$ .

Assuming that the instantaneous harmonic currents are zero  
at the beginning and at the end of the carrier cycle, the  
( $\alpha-\beta$ ) and ( $x-y$ ) harmonic stator currents per-carrier cycle can be  
calculated as follows [20], [22], [23]:

$$\begin{aligned}\tilde{i}_{s\alpha\beta} &= \frac{1}{\sigma L_s} \int_{NT_s}^{(N+1)T_s} (V_{s\alpha\beta k} - v_{s\alpha\beta}^*) dt \\ \tilde{i}_{sxy} &= \frac{1}{L_{lsxy}} \int_{NT_s}^{(N+1)T_s} (V_{sxy k}) dt.\end{aligned}\quad (12)$$

In (12),  $V_{s\alpha\beta k}$  and  $V_{sxy k}$  are the inverter output voltage  
vectors of the  $k$ th state. They change according to the selected  
switching sequence, since for high  $f_s/f_e$  values, the  $v_{s\alpha\beta}^*$  term  
can be assumed as constant within a carrier cycle. Thus, the  
above integral can be calculated in a closed form.

Because the harmonic current and harmonic flux are only  
different in scale, and in order to eliminate the need for  
load parameters in (12), the harmonic flux trajectories can  
be investigated. Nevertheless, the ( $x-y$ ) current components  
are limited by the stator leakage inductance  $L_{lsxy}$ , which de-  
pends on the coil pitch of the stator windings [10]. Conse-  
quently, the harmonic characteristics of the VSI feeding DSIM  
should be investigated with the introduction of the coefficient  
 $k_{\sigma xy} = \sigma L_s / L_{lsxy}$ , which is necessary to evaluate and com-  
pare the performances of the PWM techniques. So, employ-  
ing (12) and normalizing with respect to  $\lambda_b$ , the per-carrier  
cycle rms value of the normalized harmonic current can be  
calculated with:

$$\begin{aligned}\tilde{i}_{srms}^2(m, \theta) &= \left(\frac{\lambda_b}{\sigma L_s}\right)^2 \frac{1}{T_s} \int_{NT_s}^{(N+1)T_s} \left(\tilde{\lambda}_{s\alpha\beta}^2 + k_{\sigma xy}^2 \tilde{\lambda}_{sxy}^2\right) dt \\ &= \left(\frac{\lambda_b}{\sigma L_s}\right)^2 \left(\tilde{\lambda}_{s\alpha\beta rms}^2(m, \theta) + k_{\sigma xy}^2 \tilde{\lambda}_{sxy rms}^2(m, \theta)\right) \\ &= \left(\frac{\lambda_b}{\sigma L_s}\right)^2 \left(\tilde{\lambda}_{srms}^2(m, \theta)\right)\end{aligned}\quad (13)$$

where  $\lambda_b = 2\sqrt{3}V_{dc}T_s/\pi$ ,  $\tilde{\lambda}_{s\alpha\beta} = \sigma L_s \tilde{i}_{s\alpha\beta}$ , and  $\tilde{\lambda}_{sxy} =$   
 $L_{lsxy} \tilde{i}_{sxy}$

TABLE II  
SWITCHING FREQUENCY REDUCTION COEFFICIENT

N <sup>o</sup>	SVPWM Techniques	$k_f$	$f_s$
1	C6 $\phi$ SVPWM12	1	
2	D6 $\phi$ SVPWM12-A	2/3	
3	D6 $\phi$ SVPWM12-B1	1/2	
4	D6 $\phi$ SVPWM12-B2	5/12	$f_s = \frac{1}{k_f} \cdot f_{sw}$
5	C6 $\phi$ SVPWM24	1	
6	D6 $\phi$ SVPWM24-B1	5/6	
7	D6 $\phi$ SVPWM24-B2	2/3	

The per-fundamental cycle rms value of the harmonic current determines the waveform quality and harmonic losses. Averaging (13) over a fundamental period results in the global harmonic current calculation as follows:

$$\begin{aligned}
 \tilde{I}_{sfrms}^2(m) &= \left( \frac{\lambda_b}{\sigma L_s} \right)^2 \frac{1}{2\pi} \int_{2\pi} \tilde{\lambda}_{sfrms}^2(m, \theta) d\theta \\
 &= \left( \frac{\lambda_b}{\sigma L_s} \right)^2 \left( \tilde{\lambda}_{s\alpha\beta frms}^2(m) + k_{\sigma xy}^2 \tilde{\lambda}_{sxy frms}^2(m) \right) \\
 &= \left( \frac{\lambda_b}{\sigma L_s} \right)^2 \tilde{\lambda}_{sfrms}^2(m). \quad (14)
 \end{aligned}$$

The above integral yields a polynomial function of the modulation index  $m$ . As an example, the per-fundamental cycle rms normalized harmonic flux  $\tilde{\lambda}_{sfrms}$  was calculated for all the discussed PWM techniques. This results in  $m$  dependent analytical formulas summarized in Appendix C.

### B. Performance Comparison

For comparison purposes, the harmonic current analysis is performed at the same average switching frequency  $f_{sw}$  for all the PWM techniques. Therefore, a switching frequency reduction coefficient  $k_f$  is introduced for each PWM technique according to Table II. This coefficient can be determined from the ratio of the discontinuous to the continuous PWM techniques regarding the number of commutations of all legs during one sampling period. The curves of the per-fundamental cycle normalized rms harmonic flux for all the discussed PWM techniques have been plotted as a function of modulation index  $m$ , as shown in Fig. 7. It is clear that the rms value of the harmonic flux varies with the PWM technique used and according to the selected switching sequences. These curves show that the D6  $\phi$  SVPWM12-A has practically the best performance at a low modulation index range, while the D6  $\phi$  SVPWM12-B1 (B2) exhibits the best performance in the high modulation index range. However, as the modulation index increases, the C6  $\phi$  SVPWM12 performance rapidly degrades compared to the C6  $\phi$  SVPWM24 of the proposed 24-sector PWM scheme, which reveals excellent performance over the whole voltage range. While the D6  $\phi$  SVPWM24-B1-(B2) PWM strategies present harmonic characteristics similar to the ones obtained with the D6  $\phi$  SVPWM12-A-(B1) and (B2) strategies, the

proposed 24-sector PWM techniques allow a sampling frequency increase and as a result, the switching frequency can be increased by a factor of two as compared to the 12-sector PWMs. Therefore, significant harmonic current reductions can be achieved as shown in Fig. 7(h) for the worst case, when  $k_{\sigma xy} = 10$ .

It should be noted that discontinuous PWM techniques allow a higher sampling rate selection and can be applied in a high voltage range, while continuous ones are advantageous in the low voltage range. In addition, an optimal PWM scheme can be obtained with a transition between these SVPWM strategies to allow rms harmonic current minimization over the whole voltage range. The intersection points define the optimal transition between different PWM techniques.

Finally, a careful look at D6  $\phi$  SVPWM12-B1 in Fig. 4(c) shows that during one switching period  $T_s$ , two inverter legs have commutations twice. D6  $\phi$  SVPWM12-B2 in Fig. 4(d) shows that one inverter leg has commutations twice. This is never the case for D6  $\phi$  SVPWM24-B1 and B2. Therefore, 12-sector discontinuous PWMs have a maximum instantaneous switching frequency twice as big as in the case of 24-sector discontinuous PWMs. This fact has an impact on inverter switching losses [14], [20]. While it is not the aim of this paper to evaluate the performance of PWM techniques in terms of inverter switching and conduction losses, it can be expected that the 24-sector discontinuous PWMs will have a better performance than the 12-sector ones. Further works on switching and conduction losses are in progress and will be reported in a subsequent paper.

## V. EXPERIMENTAL RESULTS

To confirm the feasibility of the proposed SVPWM techniques over the entire voltage range under  $V/f$  control, a set of experiments are carried out. The experimental test bench (Fig. 8) is composed of a six-phase VSI feeding a 15 kW DSIM prototype, and the whole control algorithm is tested on a dSPACE DS1104 controller board. The original 320F240 firmware does not allow the change in PWM compare registers and action registers many times during a period. So, to allow four changes within PWM period  $T_s$ , the flashed firmware is reprogrammed [15], [24]. Hence, it is possible to implement the 12-sector PWM techniques.

On the contrary, for the proposed 24-sector PWM strategies, usually at most two transitions (from low to high or from high to low) occur symmetrically on the corresponding PWM outputs within a sampling period. This allows easier DSP implementation. Then the original 320F240 firmware is used with the help of specially developed user functions that allow the synchronization of six full PWM and three simple PWM simultaneously on the DS1104 DSP board.

These PWM techniques are successfully tested and the following conclusions can be drawn from these experimental results: In the case of the 12-sector PWM strategies, usually more than two transitions (from low to high or from high to low) occur on the corresponding PWM outputs. This increases the switching frequency of the inverter legs and complicates the experimental test. However, the number of transitions

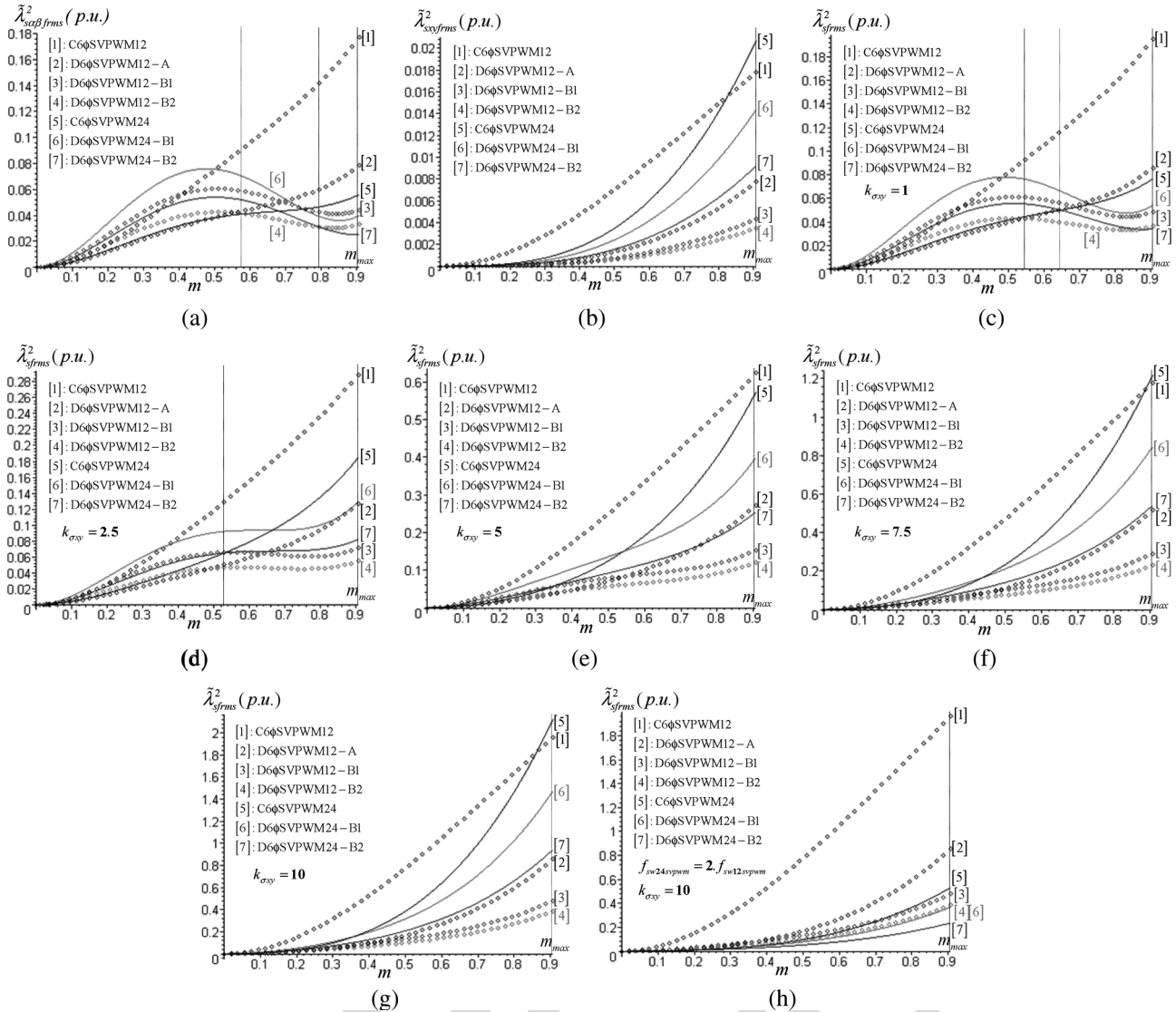


Fig. 7. Per fundamental cycle normalized rms harmonic flux as a function of modulation index  $m$ , for all the discussed PWM techniques. (a)  $(\alpha-\beta)$  rms harmonic flux. (b)  $(x-y)$  rms harmonic flux. (c), (d), (e), (f), (g) RMS harmonic flux at different leakage coupling ( $k_{\sigma xy} = 1; 2.5; 5; 7.5; 10$ ), at the same average switching frequency  $f_{sw}$ . (h) RMS harmonic flux with  $k_{\sigma xy} = 10$ , at  $f_s = 2 \cdot f_{sw}$  for the proposed 24-sector PWM techniques.

417 on the corresponding PWM outputs is reduced in the case  
418 of the proposed 24-sector PWM strategies, which decrease  
419 the switching frequency of the inverter legs and allow easy  
420 DSP implementation. In addition, for discontinuous PWM tech-  
421 niques, at least two PWM outputs remain unchanged during the  
422 entire sampling period. Therefore, the carrier frequency can be  
423 increased with harmonic losses reduction.

424 Experimental results under constant  $V/f$  control, for the  
425 cases of C6  $\phi$  SVPWM12, D6  $\phi$  SVPWM12-B2, C6  $\phi$   
426 SVPWM24, and D6  $\phi$  SVPWM24-B2 techniques are pre-  
427 sented in Fig. 9. The average switching frequency is set to  
428  $f_{sw} = 5$  kHz and the motor is running at 735 r/min with a  
429 connected load. As expected, these SVPWM techniques al-  
430 low the control of the  $(\alpha-\beta)$  and  $(x-y)$  current components  
431 simultaneously.

432 However, these experimental results demonstrate that the  
433 continuous PWM techniques produce a larger amplitude of  
434 the harmonic currents in the  $(x-y)$  plane as compared to  
435 the discontinuous ones where the amplitude of these currents

is minimized. Moreover, the phase current presents a pure  
436 sinusoidal shape and the trajectory of the  $(\alpha-\beta)$  stator cur-  
437 rent components is a circle for all these PWM techniques,  
438 confirming that these currents are controlled as well as  $(x-y)$   
439 harmonic currents. Indeed, it should be remembered that the  
440 carrier frequency can be increased by a factor of two for a 50%  
441 reduction of harmonic losses in the case of C6  $\phi$  SVPWM24,  
442 or by a factor three for a 66% reduction in harmonic losses  
443 with the D6  $\phi$  SVPWM24-B2 technique. In addition, due  
444 to the simplicity and regularity of the proposed 24-sector  
445 PWM techniques, low-cost DSPs for motor control may easily  
446 be used. 447

## VI. CONCLUSION

448  
449 In this paper, a new SVPWM technique based on the vector  
450 space decomposition suitable for six-phase VSI-fed DSIM has  
451 been presented. The switching sequences presented lead to  
452 continuous and discontinuous modulation strategies, according

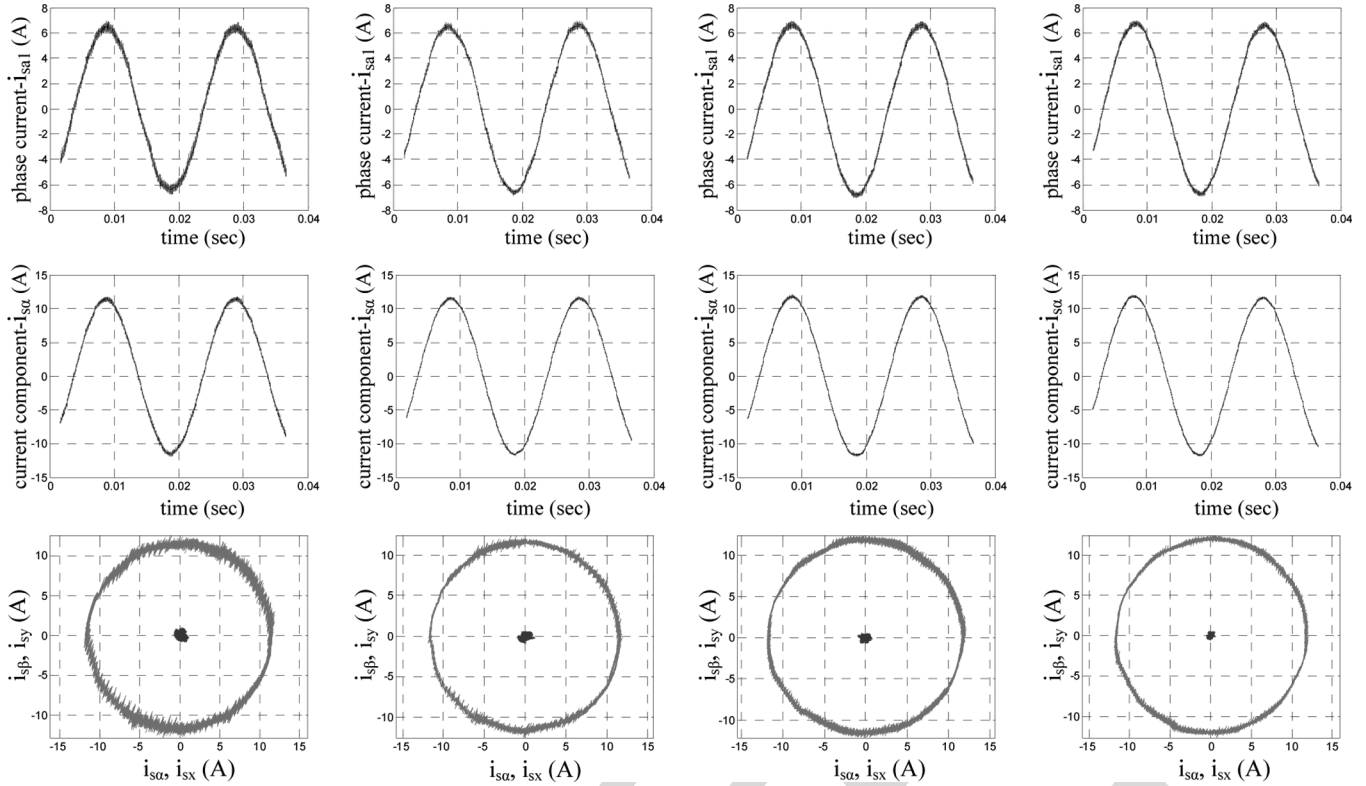


Fig. 8. Experimental test bench.

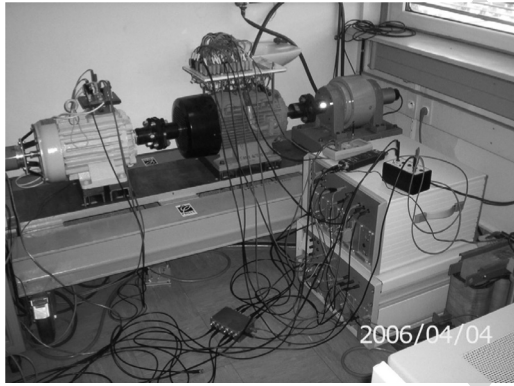


Fig. 9. Experimental results of the SVPWM techniques with the motor operating under a constant  $V/f$  control with connected load for  $f_e = 50$  Hz, at 735 r/min and for the same average switching frequency  $f_{sw}$ . From top to bottom:  $i_{sa1}$  phase current,  $i_{s\alpha}$  current component,  $(\alpha-\beta)$  and  $(x-y)$  plane current trajectories. From left to right: C6  $\phi$  SVPWM12, D6  $\phi$  SVPWM12-B2, C6  $\phi$  SVPWM24, and D6  $\phi$  SVPWM24-B2.

453 to the position of zero voltage vectors during each sampling  
454 period. It is shown that the harmonic current rms values vary  
455 according to the selected switching sequence and the voltage  
456 range. Likewise, from this point of view, the continuous PWM  
457 technique has an advantage in the low and medium voltage  
458 range, while the discontinuous PWM strategy is advantageous  
459 in the high voltage range. Thus, the combination of these  
460 strategies provides the best harmonic current performance over  
461 the whole voltage range. It has been demonstrated that the pro-  
462 posed 24-sector SVPWM techniques, while easy to implement  
463 digitally, allow a switching frequency increase with significant  
464 extra stator harmonic currents reduction.

## APPENDIX A

465

## VOLTAGE VECTORS APPLYING TIMES CALCULATION

466

The inverter output voltage vectors are represented in Figs. 3, 467  
and Fig. 5 by decimal number  $k$  equivalent to the binary number 468  
formed by the instantaneous values of the switching functions 469  
defined as: 470

$$k = K_{a1} \times 2^0 + K_{b1} \times 2^1 + K_{c1} \times 2^2 + K_{a2} \times 2^3 + K_{b2} \times 2^4 + K_{c2} \times 2^5. \quad (A1)$$

The instantaneous values of the six-phase VSI output voltage 471  
vectors  $(v_{a1}, v_{b1}, v_{c1}, v_{a2}, v_{b2}, v_{c2})$  can be determined by using 472  
the inverter connection matrix  $[Mc]$  as follows: 473

$$[v_{a1} \ v_{b1} \ v_{c1} \ v_{a2} \ v_{b2} \ v_{c2}]^T = [Mc][K_{a1} \ K_{b1} \ K_{c1} \ K_{a2} \ K_{b2} \ K_{c2}]^T \quad (A2)$$

where

474

$$[Mc] = \frac{V_{dc}}{3} \begin{bmatrix} 2 & -1 & -1 & 0 & 0 & 0 \\ -1 & 2 & -1 & 0 & 0 & 0 \\ -1 & -1 & 2 & 0 & 0 & 0 \\ \hline 0 & 0 & 0 & 2 & -1 & -1 \\ 0 & 0 & 0 & -1 & 2 & -1 \\ 0 & 0 & 0 & -1 & -1 & 2 \end{bmatrix}. \quad (A3)$$

The inverter output voltage vectors are transformed into 475  
 $(\alpha-\beta)$ ,  $(x-y)$ , and  $(o_1-o_2)$  planes by means of the transfor- 476  
mation matrix  $[Ts]^{-1}$  given in (1), as: 477

$$[v_{s\alpha k} \ v_{s\beta k} \ v_{sxk} \ v_{syk} \ v_{o1k} \ v_{o2k}]^T = [Ts]^{-1}[v_{a1} \ v_{b1} \ v_{c1} \ v_{a2} \ v_{b2} \ v_{c2}]^T \quad (A4)$$

478 For example, when the reference voltage vector is located in  
479 sector 1, voltage vectors 41, 9, 11, and 15 are selected and their  
480 equivalent binary numbers are defined as:

$$\begin{aligned} 41 &= [1 \ 0 \ 1|0 \ 0 \ 1] \\ 9 &= [0 \ 0 \ 1|0 \ 0 \ 1] \\ 11 &= [0 \ 0 \ 1|0 \ 1 \ 1] \\ 15 &= [0 \ 0 \ 1|1 \ 1 \ 1]. \end{aligned} \quad (\text{A5})$$

481 Then the  $(\alpha-\beta)$ , and  $(x-y)$  voltages can be calculated by  
482 using (A2), and (A4), as follows:

$$\begin{aligned} &\begin{bmatrix} V_{s\alpha 41} & V_{s\alpha 9} & V_{s\alpha 11} & V_{s\alpha 15} \\ V_{s\beta 41} & V_{s\beta 9} & V_{s\beta 11} & V_{s\beta 15} \\ V_{sx 41} & V_{sx 9} & V_{sx 11} & V_{sx 15} \\ V_{sy 41} & V_{sy 9} & V_{sy 11} & V_{sy 15} \end{bmatrix} \\ &= \frac{V_{dc}}{2\sqrt{3}} \begin{bmatrix} 2 + \sqrt{3} & 2 + \sqrt{3} & 1 + \sqrt{3} & \sqrt{3} \\ -1 & 1 & 1 + \sqrt{3} & 1 \\ 2 - \sqrt{3} & 2 - \sqrt{3} & 1 - \sqrt{3} & -\sqrt{3} \\ -1 & 1 & 1 - \sqrt{3} & 1 \end{bmatrix}. \end{aligned} \quad (\text{A6})$$

483 The voltage vectors applying times:  $t_1$ ,  $t_2$ ,  $t_3$  and  $t_4$  are  
484 obtained as:

$$\begin{aligned} \begin{bmatrix} t_1 \\ t_2 \\ t_3 \\ t_4 \end{bmatrix} &= \begin{bmatrix} V_{s\alpha 41} & V_{s\alpha 9} & V_{s\alpha 11} & V_{s\alpha 15} \\ V_{s\beta 41} & V_{s\beta 9} & V_{s\beta 11} & V_{s\beta 15} \\ V_{sx 41} & V_{sx 9} & V_{sx 11} & V_{sx 15} \\ V_{sy 41} & V_{sy 9} & V_{sy 11} & V_{sy 15} \end{bmatrix}^{-1} \begin{bmatrix} v_{s\alpha}^* T_s \\ v_{s\beta}^* T_s \\ v_{sx}^* T_s \\ v_{sy}^* T_s \end{bmatrix} \\ t_0 &= T_s - (t_1 + t_2 + t_3 + t_4). \end{aligned} \quad (\text{A7})$$

485 Substituting (A6) in (A7), the applying times can be calcu-  
486 lated as follows:

$$\begin{aligned} \begin{bmatrix} t_1 \\ t_2 \\ t_3 \\ t_4 \end{bmatrix} &= \frac{T_s}{2V_{dc}} \begin{bmatrix} 1 & -\sqrt{3} & -1 & -\sqrt{3} \\ \sqrt{3}-1 & \sqrt{3}-1 & \sqrt{3}+1 & \sqrt{3}+1 \\ 0 & 2 & 0 & v-2 \\ -(\sqrt{3}-2) & -1 & -(\sqrt{3}+2) & 1 \end{bmatrix} \begin{bmatrix} v_{s\alpha}^* \\ v_{s\beta}^* \\ v_{sx}^* \\ v_{sy}^* \end{bmatrix}. \end{aligned} \quad (\text{A8})$$

487 With  $v_{sx}^* = v_{sy}^* = 0$ , (A8) can be written as:

$$\begin{aligned} \begin{bmatrix} t_1 \\ t_2 \\ t_3 \\ t_4 \end{bmatrix} &= \frac{T_s}{2V_{dc}} \begin{bmatrix} 1 & -\sqrt{3} \\ \sqrt{3}-1 & \sqrt{3}-1 \\ 0 & 2 \\ -(\sqrt{3}-2) & -1 \end{bmatrix} \begin{bmatrix} v_{s\alpha}^* \\ v_{s\beta}^* \end{bmatrix} = \begin{bmatrix} T_2 \\ T_5 \\ T_4 \\ -T_1 \end{bmatrix}. \end{aligned} \quad (\text{A9})$$

#### 488 APPENDIX B 489 MAXIMUM MODULATION INDEX CALCULATION

490 The maximum modulation index  $m_{\max}$  can be obtained  
491 by solving  $t_0 = T_s - (t_1 + t_2 + t_3 + t_4) = 0$ . For example in  
492 sector 1, the sum of the applying times of the active voltage  
493 vectors is calculated from (A9) as:

$$\theta \in \left[0, \frac{\pi}{12}\right] \quad t_1 + t_2 + t_3 + t_4 = \frac{T_s}{V_{dc}} v_{s\alpha}^* \quad (\text{B1})$$

494 where  $v_{s\alpha}^* = \sqrt{3}V_{1m} \cos(\theta)$ ,  $v_{s\beta}^* = \sqrt{3}V_{1m} \sin(\theta)$

$$V_{1m} = mV_{1m6\text{step}} = m2V_{dc}/\pi.$$

When

$$t_0 = 0 : T_s = t_1 + t_2 + t_3 + t_4 = 2\sqrt{3}\frac{T_s}{\pi}m \cos(\theta) \quad (\text{B2})$$

From (B2), the modulation index equation can be given as: 496

$$m = \frac{\pi}{2\sqrt{3} \cos(\theta)}. \quad (\text{B3})$$

To determine the angle  $\theta$  corresponding to  $m_{\max}$ , (B3) is 497  
derived: 498

$$\frac{dm}{d\theta} = \frac{\pi \sin(\theta)}{2\sqrt{3} \cos^2(\theta)}. \quad (\text{B4})$$

Equation (B4) is solved for  $\theta = 0$ . Thus, replacing  $\theta$  in (B3): 499

$$m_{\max} = \frac{\pi}{2\sqrt{3} \cos(0)} = \frac{\pi}{2\sqrt{3}} \approx 0.907. \quad (\text{B5})$$

#### APPENDIX C 500 ANALYTICAL FORMULAS OF THE RMS HARMONIC FLUX 501

The per-fundamental cycle rms normalized harmonic flux 502  
 $\tilde{\lambda}_{s\text{frms}}$  was calculated for all the discussed PWM techniques. 503  
Only the analytical formulas of the proposed 24-sector PWMs 504  
are presented here and the ones of the 12-sector PWMs can be 505  
found in [10]. These formulas are given below. 506

##### A. Continuous Modulation C6 $\phi$ SVPWM24 507

$$\begin{aligned} \tilde{\lambda}_{s\alpha\beta\text{frms}}^2(m) &= \frac{1}{48}m^2 + \frac{1}{144\pi^2} \\ &\quad \times (56\sqrt{3} + 63\sqrt{6} - 57\sqrt{2} - 228)m^3 \\ &\quad + \frac{1}{32\pi^3}(24\pi + 27 - 21\sqrt{3} - 8\sqrt{3}\pi)m^4 \\ \tilde{\lambda}_{sxy\text{frms}}^2(m) &= \frac{1}{144\pi^2}(63\sqrt{6} + 18 - 52\sqrt{3} - 57\sqrt{2})m^3. \end{aligned} \quad (\text{C1})$$

##### B. Discontinuous Modulation D6 $\phi$ SVPWM24-B1 508

$$\begin{aligned} \tilde{\lambda}_{s\alpha\beta\text{frms}}^2(m) &= \frac{25}{432}m^2 - \frac{25}{5184\pi^2} \\ &\quad \times (633\sqrt{2} + 408 - 56\sqrt{3} - 387\sqrt{6})m^3 \\ &\quad - \frac{25}{576\pi^3}(15\sqrt{3} + 8\sqrt{3}\pi - 24\pi - 45)m^4 \\ \tilde{\lambda}_{sxy\text{frms}}^2(m) &= \frac{25}{5184\pi^2}(63\sqrt{6} + 18 - 52\sqrt{3} - 57\sqrt{2})m^3. \end{aligned} \quad (\text{C2})$$

##### C. Discontinuous Modulation D6 $\phi$ SVPWM24-B2 509

$$\begin{aligned} \tilde{\lambda}_{s\alpha\beta\text{frms}}^2(m) &= \frac{1}{27}m^2 - \frac{1}{324\pi^2} \\ &\quad \times (129\sqrt{2} + 45\sqrt{6} + 48 - 56\sqrt{3})m^3 \\ &\quad + \frac{1}{6\pi^3}(2\pi + 3 - \sqrt{3})m^4 \\ \tilde{\lambda}_{sxy\text{frms}}^2(m) &= \frac{1}{324\pi^2}(63\sqrt{6} + 18 - 52\sqrt{3} - 57\sqrt{2})m^3. \end{aligned} \quad (\text{C3})$$

510

## REFERENCES

- 511 [1] V. T. Somasekhar, K. Gopakumar, M. R. Baiju, K. K. Mohapatra, and  
512 L. Umanand, "A multilevel inverter system for an induction motor with  
513 open-end windings," *IEEE Trans. Ind. Electron.*, vol. 52, no. 3, pp. 824–  
514 836, Jun. 2005.
- 515 [2] R. C. Portillo *et al.*, "Modeling strategy for back-to-back three-level con-  
516 verters applied to high-power wind turbines," *IEEE Trans. Ind. Electron.*,  
517 vol. 53, no. 5, pp. 1483–1491, Oct. 2006.
- 518 [3] A. K. Gupta and A. M. Khambadkone, "A space vector PWM scheme for  
519 multilevel inverters based on two-level space vector PWM," *IEEE Trans.*  
520 *Ind. Electron.*, vol. 53, no. 5, pp. 1631–1639, Oct. 2006.
- 521 [4] K. Hatua and V. T. Ranganathan, "Direct torque control schemes for  
522 split-phase induction machine," *IEEE Trans. Ind. Appl.*, vol. 41, no. 5,  
523 pp. 1243–1254, Sep./Oct. 2005.
- 524 [5] Y. Zhao and T. A. Lipo, "Space vector PWM control of dual three-phase  
525 induction machine using vector space decomposition," *IEEE Trans. Ind.*  
526 *Appl.*, vol. 31, no. 5, pp. 1100–1109, Sep./Oct. 1995.
- 527 [6] M. A. Abbas, R. Christen, and T. M. Jahns, "Six-phase voltage source  
528 inverter driven induction motor," *IEEE Trans. Ind. Appl.*, vol. IA-20, no. 5,  
529 pp. 1251–1259, Sep./Oct. 1984.
- 530 [7] D. Hadiouche, H. Razik, and A. Rezzoug, "On the modeling and design  
531 of dual-stator windings to minimize circulating harmonic currents for VSI  
532 fed AC machines," *IEEE Trans. Ind. Appl.*, vol. 40, no. 2, pp. 506–515,  
533 Mar./Apr. 2004.
- 534 [8] A. R. Muñoz and T. A. Lipo, "Dual stator winding induction machine  
535 drive," *IEEE Trans. Ind. Appl.*, vol. 36, no. 5, pp. 1369–1379,  
536 Sep./Oct. 2000.
- 537 [9] K. Gopakumar, V. T. Ranganathan, and S. R. Bhat, "Split-phase induction  
538 motor operation from PWM voltage source inverter," *IEEE Trans. Ind.*  
539 *Appl.*, vol. 29, no. 5, pp. 927–932, Sep./Oct. 1993.
- 540 [10] D. Hadiouche, L. Baghli, and A. Rezzoug, "Space vector PWM  
541 techniques for dual three-phase AC machine: Analysis, performance  
542 evaluation, and DSP implementation," *IEEE Trans. Ind. Appl.*, vol. 42,  
543 no. 4, pp. 1112–1122, Jul./Aug. 2006.
- 544 [11] R. Bojoi, M. Lazzari, F. Profumo, and A. Tenconi, "Digital field-oriented  
545 control for dual three-phase induction motor drives," *IEEE Trans. Ind.*  
546 *Appl.*, vol. 39, no. 3, pp. 752–760, May/Jun. 2003.
- 547 [12] K. K. Mohapatra, R. S. Kanchan, M. R. Baiju, P. N. Tekwani, and  
548 K. Gopakumar, "Independent field-oriented control of two split-phase  
549 induction motors from a single six-phase inverter," *IEEE Trans. Ind.*  
550 *Electron.*, vol. 52, no. 5, pp. 1372–1382, Oct. 2005.
- 551 [13] W. Tiejun, G. Chenglin, C. Yongbing, and J. Xiaoyi, "Research on har-  
552 monics of multiphase induction motors," in *Proc. IEEE IEMDC*, Antalya,  
553 Turkey, May 3–5, 2007, pp. 1524–1528.
- 554 [14] J. W. Kolar, H. Ertl, and F. C. Zach, "Influence of the modulation method  
555 on the conduction and switching losses of a PWM converter system,"  
556 *IEEE Trans. Ind. Appl.*, vol. 27, no. 6, pp. 1063–1075, Nov./Dec. 1991.
- 557 [15] K. Marouani, L. Baghli, D. Hadiouche, A. Kheloui, and A. Rezzoug,  
558 "Discontinuous SVPWM techniques for double star induction motor  
559 drive control," in *Proc. IEEE IECON*, Paris, France, Nov. 6–10, 2006,  
560 pp. 902–907.
- 561 [16] G. K. Singh, K. Nam, and S. K. Lim, "A simple indirect field-oriented  
562 control scheme for multiphase induction machine," *IEEE Trans. Ind.*  
563 *Electron.*, vol. 52, no. 4, pp. 1177–1184, Aug. 2005.
- 564 [17] D. C. Lee and G. M. Lee, "Linear control of inverter output voltage in  
565 overmodulation," *IEEE Trans. Ind. Electron.*, vol. 44, no. 4, pp. 590–592,  
566 Aug. 1997.
- 567 [18] S. R. Bowes and Y. S. Lai, "The relationship between space-vector mod-  
568 ulation and regular-sampled PWM," *IEEE Trans. Ind. Electron.*, vol. 44,  
569 no. 5, pp. 670–679, Oct. 1997.
- 570 [19] O. Ojo, "The generalized discontinuous PWM scheme for three-phase  
571 voltage source inverters," *IEEE Trans. Ind. Electron.*, vol. 51, no. 6,  
572 pp. 1280–1289, Dec. 2004.
- 573 [20] A. M. Hava, R. J. Kerkman, and T. A. Lipo, "Simple analytical and graph-  
574 ical methods for carrier-based PWM-VSI drives," *IEEE Trans. Power*  
575 *Electron.*, vol. 14, no. 1, pp. 49–61, Jan. 1999.
- 576 [21] S. Ogasawara, H. Akagi, and A. Nabae, "A novel PWM scheme of voltage  
577 source inverters based on space vector theory," in *Proc. EPE*, Aachen,  
578 Germany, Oct. 1989, pp. 1197–1202.
- 579 [22] H. W. van der Broeck, H. C. Skudelyni, and G. V. Stanke, "Analysis and  
580 realization of a pulsewidth modulator based on voltage space vectors,"  
581 *IEEE Trans. Ind. Appl.*, vol. 24, no. 1, pp. 142–150, Jan./Feb. 1988.
- 582 [23] J. Holtz and B. Beyer, "Optimal pulse width modulation for AC servos  
583 and low-cost industrial drives," *IEEE Trans. Ind. Appl.*, vol. 30, no. 4,  
584 pp. 1039–1047, Jul./Aug. 1994.
- 585 [24] *TMS320F/C240 DSP Controllers Reference Guide, Peripheral and Spe-*  
586 *cific Devices*, Texas Instruments, Dallas, TX, 1999. Literature Number  
587 SPRU161C.



**Khoudir Marouani** was born in 1972. He received 588 **AQ1**  
the Degree of Engineer in automatics and the Degree 589  
of Magister in electrical engineering from the Poly- 590  
technic Military School (EMP), Algiers, Algeria, in 591  
1996 and 2000, respectively, where he is currently 592  
working toward the Ph.D. degree in the Electrical 593  
Engineering Laboratory. 594

He is currently working as a Research and Teach- 595  
ing Assistant with the Electrical Engineering Lab- 596  
oratory, EMP. His research interests include power 597  
electronics, electrical drives and active power filters. 598



**Lotfi Baghli** was born in 1971. He received the 599 **AQ2**  
Electrical Engineering Diploma degree (with honors) 600  
from the Ecole Nationale Polytechnique, Algiers, 601  
Algeria, in 1989, and the DEA degree in electri- 602  
cal engineering from the Université Henri Poincaré, 603  
Nancy, France, in 1995 and 1999, respectively. 604

He is currently a Lecturer at IUFM de Lorraine 605 **AQ3**  
and a member of Groupe de Recherche en Elec- 606  
trotechnique et Electronique de Nancy, Nancy. His 607  
works concern digital control using DSP, PSO and 608  
genetic algorithms applied to the control and identi- 609  
fication of electrical machines. 610



**Djafar Hadiouche** was born in 1974. He received 611 **AQ4**  
the Ph.D. degree in electrical engineering from the 612  
University Henri Poincaré, Nancy, France, in 2001. 613

Until 2002, he was Assistant Lecturer in the 614  
same university and did research in the laboratory 615  
of the "Groupe de Recherche en Electrotechnique 616  
et Electronique de Nancy," Nancy. Since 2003, he 617  
has been a Motion Specialist Engineer with GE 618  
Fanuc Automation Solutions Europe, Echternach, 619  
Luxembourg. His main tasks include servosizing, 620  
tools and motion programs development, electronic 621  
cam profiling and motion technical training. His main research interests concern 622  
multiphase ac machines, their modeling, identification, pulsewidth modulation 623  
techniques, and vector control. 624

Dr. Hadiouche received the Best Prize Paper Award from the Electric 625  
Machine Committee at the 2001 IEEE IAS Annual Meeting. 626



**Abdelaziz Kheloui** was born in 1969. He received 627 **AQ5**  
the M.Sc.Eng. degree from the Ecole Nationale 628  
d'ingénieurs et Techniciens d'Algérie, Algiers, 629  
Algeria, in 1990, and the Ph.D. degree in electrical 630  
engineering from the Institut National Polytechnique 631  
de Lorraine, Nancy, France, in 1994. 632

Since 1994, he has been a Researcher and a 633  
Teacher at the electrical engineering laboratory of 634  
the Polytechnic Military School, Algiers, Algeria. 635  
His current research interests are control of electrical 636  
drives and power electronics. 637



**Abderrezak Rezzoug** was born in 1948. He received 638 **AQ6**  
the Electrical Engineer degree, Dr. Ing. diploma, 639  
and Ph.D. degree from ENSEM Institut National 640 **AQ7**  
Polytechnique de Lorraine, Nancy, France, in 1972, 641  
1979, and 1987, respectively. 642

He is currently a Professor in electrical engineer- 643  
ing at the Université Henri Poincaré, Nancy. As a 644  
member of the Groupe de Recherche en Electrotech- 645  
nique et Electronique de Nancy, Nancy, his main 646  
areas of research concern electrical machines, their 647  
identification, diagnostic and control, and supercon- 648  
ducting applications. 649

## AUTHOR QUERIES

AUTHOR PLEASE ANSWER ALL QUERIES

AQ1 = “1972” was assumed as the author’s birth year. Please check if appropriate.

AQ2 = “1971” was assumed as the author’s birth year. Please check if appropriate.

AQ3 = Please provide the expanded form of the acronym “IUFM”.

AQ4 = “1974” was assumed as the author’s birth year. Please check if appropriate.

AQ5 = “1969” was assumed as the author’s birth year. Please check if appropriate.

AQ6 = “1948” was assumed as the author’s birth year. Please check if appropriate.

AQ7 = Please provide the expanded form of the acronym “ENSEM”.

Note: Figure citations were renumbered. The original sequence was 1-2-3-4-5-6-7-9-8.

END OF ALL QUERIES

LEEE  
PROOF